

Style-Aware Gloss Control for Generative Non-Photorealistic Rendering

Santiago Jimenez-Navarro*, Belen Masia, Ana Serrano

University of Zaragoza – I3A, Spain

Abstract

Humans can infer material characteristics of objects from their visual appearance, and this ability extends to artistic depictions, where similar perceptual strategies guide the interpretation of paintings or drawings. Among the factors that define material appearance, gloss, along with color, is widely regarded as one of the most important, and recent studies indicate that humans can perceive gloss independently of the artistic style used to depict an object. To investigate how gloss and artistic style are represented in learned models, we train an unsupervised generative model on a newly curated dataset of painterly objects designed to systematically vary such factors. Our analysis reveals a hierarchical latent space in which gloss is disentangled from other appearance factors, allowing for a detailed study of how gloss is represented and varies across artistic styles. Building on this representation, we introduce a lightweight adapter that connects our style- and gloss-aware latent space to a latent-diffusion model, enabling the synthesis of non-photorealistic images with fine-grained control of these factors. We compare our approach with previous models and observe improved disentanglement and controllability of the learned factors.

Keywords: Non-photorealistic rendering, Appearance perception, Dimensionality reduction, Intuitive editing

1. Introduction

Visual perception plays a fundamental role in everyday life. We constantly evaluate the appearance of surrounding objects in order to interact with them effectively, either by not stepping on a wet floor, or by not touching a sharp blade. While such processing is largely automatic for humans, the perceived appearance of materials arises from a complex interplay of factors such as shape, illumination, and motion [1, 2, 3]. This interaction is not yet fully understood, and remains an active area of research [4, 5, 6]. For example, a same golden ring may appear shinier under the bright spotlights of a jewelry display than under dull lighting on a tabletop. Beyond photorealistic scenes, this is also relevant in non-photorealistic renditions (e.g., paintings), where an

additional factor may influence appearance perception: the style with which they are depicted. Among the different dimensions of material appearance, gloss is one of the most relevant attributes, together with color, and has therefore received particular attention in perception studies [7, 2]. Recent studies suggest that the human brain is able to disambiguate gloss from style, relying on similar visual cues across different media [8, 9, 10]. Because gloss is a key component of material appearance and may be influenced by the painting style, it is a particularly relevant attribute for studying appearance in non-photorealistic images. In this work, we investigate whether a generative network trained on stylized renditions of objects can, without supervision, learn a hierarchical latent representation in which gloss is separated from other appearance factors such as style (Sec. 3). This representation allows direct analysis of how visual factors are internally organized (Sec. 4), and provides a basis for controlled manipulation of gloss in images.

Building on the learnt representation, we next explore its potential for image synthesis (Sec. 5). Generative models based on latent diffusion denoising processes are, together with flow-based models, the current state of the art in image synthesis [11]. While these models can produce high-quality images, a fine-

*Corresponding Author. Address: University of Zaragoza, Department of Computer Science and Systems Engineering (DIIS), Zaragoza, Spain

Email addresses: s.jimenez@unizar.es (Santiago Jimenez-Navarro), bmasia@unizar.es (Belen Masia), anase@unizar.es (Ana Serrano)

URL: <https://santiagojn.github.io/> (Santiago Jimenez-Navarro), <https://webdiis.unizar.es/~bmasia/> (Belen Masia), <https://ana-serrano.github.io/> (Ana Serrano)

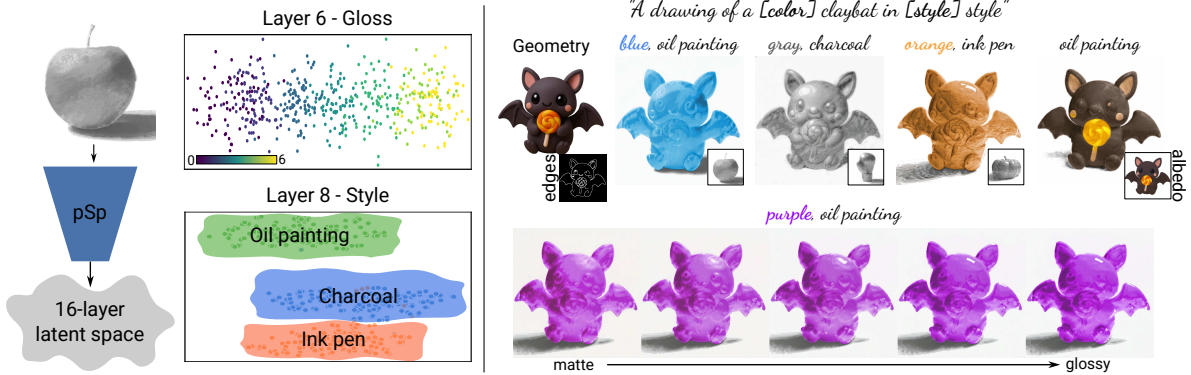


Figure 1: *Left*: We train a pSp-StyleGAN2 pipeline that learns a 16-layer latent space where appearance factors such as gloss and artistic style emerge in a disentangled and hierarchical manner. Specific layers specialize in different attributes, e.g., Layer 6 captures gloss and Layer 8 captures style. *Right*: This learned space enables intuitive control of appearance. Given a reference geometry (edges) and optional albedo map, the user can employ our diffusion-based pipeline to transfer the gloss and style of an input drawing (inset) to new objects, or traverse the gloss dimension to obtain predictable variations from matte to glossy while keeping other factors stable.

grained control of the output is difficult, and represents an active area of research [12, 13, 14, 15]. Conversely, GAN-based models have been extensively studied in the literature, where their favorable latent-space properties (e.g. interpretability, traversability, and continuity) have been exploited to identify editing directions that enable an intuitive manipulation of high-level image features [16, 17]. However, these approaches are inherently limited by the reduced generative capacity of the GAN’s generator. Inspired by prior work on controlled generation [18, 19, 20], we explore how our latent space can be exploited to enable precise manipulation of style and gloss within diffusion models, two appearance factors that are normally hard to define through text prompts alone (Sec. 5, Fig. 12).

Overall, our latent representation contains an interpretable and disentangled encoding of gloss and other perceptual factors present in stylized images and enables fine-grained control of a diffusion pipeline. Thus, our main contribution is a detailed analysis of how style influences the internal representation of visual attributes within a hierarchical, learning-based network trained without explicit supervision, revealing the emergence of a dedicated gloss dimension. Building on this analysis, we leverage the learned representation to enable diffusion-based image synthesis with fine-grained appearance control, achieving a level of gloss manipulation that is not attainable with existing style-transfer or general-purpose diffusion methods.

Our trained model and code will be made public soon. We will also release our dataset, comprised of non-photorealistic renditions of objects depicted under different styles and levels of gloss.

2. Related Work

2.1. Image Stylization in Non-photorealistic Rendering

Non-photorealistic rendering (NPR) refers to computer-graphics techniques that deliberately depart from photorealism to produce images with a hand-crafted or illustrative appearance. Rather than reproducing the physical accuracy of light transport, NPR methods aim to convey the content of a scene through artistic or stylized depiction. A central task in this area is image stylization, where a source image is transformed to match a chosen artistic style. Early approaches address this task by explicitly defining brushstrokes or procedural painting rules. While effective, these analytical methods are typically slow, non-intuitive, and require manual parameter tuning [21, 22], which limits usability [23].

Since the introduction of Neural Style Transfer by Gatys et al. [24], a variety of approaches have been developed to automatically apply a reference style to an image. Early CNN-based methods [24, 25] rely on high-level features extracted from pretrained networks such as VGG [26]. Later, StyleGAN-based models employed the classic *min–max* training of generator and discriminator to produce more realistic and diverse results [27, 28]. Most recently, diffusion-based models have achieved state-of-the-art performance in terms of image quality, robustness, and diversity [29, 30]. A key challenge of this last type of models is their limited controllability, which has been mitigated with reasonable success by auxiliary networks that allow finer conditioning during synthesis [12, 13, 14, 15]. For a more detailed discussion on the taxonomy and evolution of

the aforementioned methods, we refer the reader to the survey by Wang et al. [31].

In our work, we condition a diffusion model on artistic styles represented in the W^+ latent space of StyleGAN, a representation that offers both expressivity and controllability [18, 19]. Our focus is on capturing style and gloss levels independently and simultaneously, extending prior efforts in NPR stylization. The closest related work to ours is that of Subias et al. [32], who introduced a diffusion pipeline for text-driven stylization. While their approach improves flexibility in stylization, it still lacks explicit disentanglement of appearance factors and therefore cannot provide the predictable, continuous control that our method enables.

2.2. Perception in Non-photorealistic Rendering

Artistic depictions have long served as a tool for studying human visual perception. To represent real scenes, artists frequently use deliberate abstractions that allow them to effectively convey visual attributes of objects without adhering to strict photorealism [9, 8, 33]. Although some early studies reported differing interpretations [34], more recent work supports the view that the human visual system relies on similar cues to judge material properties across different media [8, 9, 10], allowing systematic studies to extend beyond strictly photorealistic images.

Non-photorealistic depictions have been used to investigate a variety of material properties, including transparency [35], translucency [36], and specific materials such as fabrics [37, 38]. Among these attributes, gloss has received particular attention in non-photorealistic settings [9, 39, 40, 32], as gloss, together with color, is widely regarded as one of the most important attributes of material appearance [7, 2]. In this work, we investigate how attributes related to different painting techniques—charcoal, oil painting, and ink pen—are naturally organized in the inner layers of a generative model. The closest studies on this aspect are those of Zhao et al. [41] and Elgammal et al. [42]. However, both of them focus on interpreting a low-dimensional embedding space and its relation to specific painters or creation years, rather than studying how information about painting techniques can be captured within a hierarchical generator.

2.3. Generative Models and Human Perception

Humans excel at estimating physical properties of materials by sight. This core ability allows us to interact effectively with our surroundings, assessing whether a certain object is edible, slippery, or sharp [43, 2, 3]. This

material perception results from a complex interplay between intrinsic and extrinsic factors [1, 4]. However, it is argued that the brain does not explicitly recover the physical reflectance parameters of a surface, but instead relies on statistical generative representations to perceive material appearance [44].

Learning-based generative models are increasingly used to investigate the neural mechanisms underlying human visual perception [45, 46]. As discussed in Sec. 2.2, gloss perception has been a common benchmark for assessing the correspondence between artificial networks and human visual judgments [47, 48, 49]. Other factors, such as translucency [50], viscosity [51] and refractive or reflective properties [52] have also been explored in this context. Demonstrating that these models can simulate human perception requires more than reproducing correct judgments; it also entails showing that they exhibit similar failure patterns. Building on this idea, a growing line of work uses generative models to study visual illusions, examining how the visual system can be misled by specific image statistics [53, 54, 55]. Such studies help identify the internal mechanisms that lead to systematic misperceptions and can even guide the creation of new illusions [55].

In this work, we examine the features that naturally emerge within a StyleGAN2-ADA generator [56] and analyze how their internal organization relates to visual representations of perceptual features.

3. Disentanglement of Style and Gloss in W^+ space

Our goal is to investigate how gloss is represented in a generative model specialized for non-photorealistic rendering across a set of styles. Building on the incremental process of hierarchical generators such as StyleGAN2 [57], we evaluate whether interpretable and informative dimensions of material appearance can naturally emerge in a model trained without explicit supervision and, in that case, how and why they are organized in that manner. While the use of multiple artistic styles introduces arbitrariness in the representations (e.g., of a given gloss level), it also allows us to study if factors that evoke the sense of gloss can be shared across different styles.

3.1. Preliminaries

We rely on an unsupervised learning-based approach to study how gloss perception is affected by artistic styles in non-photorealistic rendering. In this section, we give background on the neural architectures that form the final pipeline, and the dataset specially created for this task.

Unsupervised approaches have proven to be useful for providing insights on how the human visual system may perceive complex stimuli from the real world [58, 47]. In this work, we use a version of the well known Generative Adversarial Network (GAN) [59], namely StyleGAN2-ADA [56], together with a style encoder [60] to easily project samples into the latent space.

StyleGAN2-ADA. The StyleGAN architecture [61] represented a major step forward on the interpretability and explainability of GAN-synthesized images by redesigning the generator component. Authors propose embedding the traditional, normally-distributed latent representation $z \in Z$ to an intermediate $w \in W$, which is more suitable to represent the distribution of input data, allowing a more disentangled representation of the factors of variation. This is achieved by a learned non-linear mapping network $f : Z \rightarrow W$, where the resulting w is injected to each convolutional layer of the synthesis network via affine transformations.

StyleGAN2 [57] revised the synthesis architecture of its predecessor to remove some characteristic artifacts, improve general image quality, and facilitating the inversion task [62]. Finally, StyleGAN2-ADA [56] introduces an Adaptive Discriminator Augmentation mechanism that allows training a model from scratch with only *a few thousand training images*.

In this work we use the StyleGAN2-ADA architecture [56] (henceforth denoted as StyleGAN2 for simplicity) for the aforementioned benefits in terms of disentanglement and interpretability of results. Furthermore, ADA improves training stability when data are scarce, reducing the need to gather a very large set of high-quality painterly depictions.

pixel2style2pixel (pSp) encoder. GAN-based methods have shown a great capability to generate high-quality and varied images in an unconditioned way [62], closely approximating the distribution of datasets of varied size and complexity [63]. Furthermore, it has been shown that information tends to naturally organize in a semantically-meaningful way throughout the different hierarchical levels of the generator network [64, 65]. This opens the door to an intuitive and predictable editing of some interpretable factors of the GAN-generated images, by traversing the latent space Z (or any of its variants) [66, 67].

In order to perform this editing with an unknown image x , it is first necessary to estimate how x is represented in the latent space, which can be formulated as the function $I : x \rightarrow z^*$. This constitutes a complex inverse problem due to the non-convexity of the generator network. The literature contains an extensive number of approaches to this GAN inversion prob-

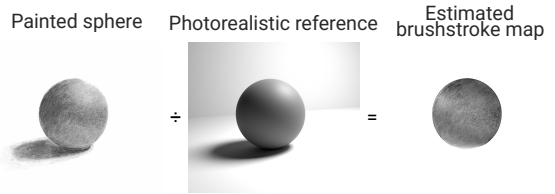


Figure 2: Example of brushstroke map extraction for a matte sphere painted in charcoal style. Artist-painted reference (left), corresponding photorealistic rendering (middle), and the estimated brushstroke map extracted from the pair (right).

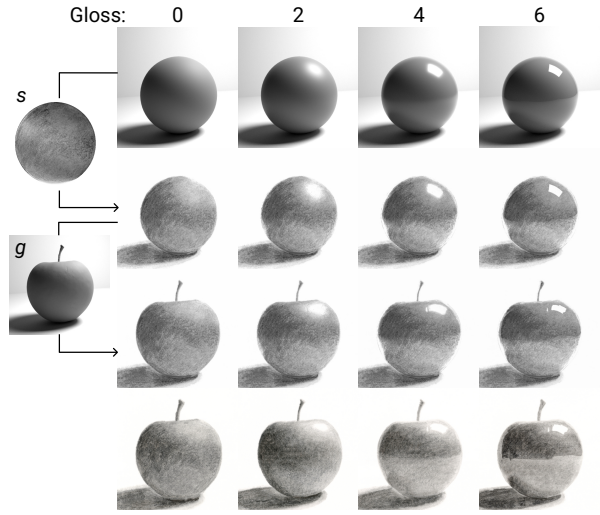


Figure 3: Application of the brushstroke map s to generate controlled style-guidance samples. From top to bottom rows, we show 1) the photorealistic reference spheres with gradually varying roughness; 2) the stylized spheres using the estimated brushstroke map s ; 3) the result of applying StyLit to the reference geometry g ; and 4) the corresponding samples from the original Subias dataset [32]. Note the more controlled and continuous increment of gloss of our samples when compared with the reference.

lem, which can be categorized as (i) optimization-based, where z^* is estimated through a costly but precise optimization process [27], (ii) learning-based techniques which create an auxiliary encoder network that approximates I [60, 68], similar to an autoencoder [69], and (iii) hybrid methods that combine both [70]. We use a learning-based approach, namely pSp [60], since it is able to perform inversion in a single forward pass, and it has been shown that these models can achieve better disentanglement and informativeness capabilities than the original Z [67]. The pSp encoder expands the original StyleGAN’s W space (single 512-dimensional embeddings) to an extended $W+$ space (one independent 512-dimensional style vector per generator layer), where feature maps are extracted using a small fully convolutional network, *map2style*.

3.2. A Dataset for Stylized Gloss

Although datasets for studying glossiness are common in photorealistic scenarios, their availability in NPR is limited. Existing datasets either offer limited control over generative factors [40, 71] or are too small to train an unsupervised generative model [9]. A recent work from Subias et al. [32] introduced a varied and relatively controlled dataset of 1,336,272 painterly depictions generated with StyLit [72]. The creation of this dataset involved two stages. First, Subias et al. produced an original collection of reference pairs consisting of physically rendered spheres with controlled gloss levels and their corresponding artist-painted versions in different artistic styles. Second, they used these painted spheres as style exemplars to transfer the appearance to a wide variety of geometries with StyLit, yielding the final large-scale set. While the dataset is large-scale and offers controlled variability in generative factors, its direct use represents a major issue in our setup: because different gloss levels in the references come from different hand-painted spheres, a trained unsupervised model is likely to learn differences in brushstrokes rather than actual gloss variations (Fig. 3). Indeed, a preliminary experiment with our architecture showed early signs of clustering images by stroke patterns rather than gloss level. Therefore, for our purposes, appearance references (painted spheres) in a given style must be invariant with respect to brushstroke patterns.

For this purpose, we reprocess the reference pairs provided by Subias et al. (the physically rendered spheres with controlled gloss levels and their artist-painted counterparts). Inspired by the work of Litwinowicz [73], our goal is to create a brushstroke map s that contains information about the artistic style. For each style, we select the painted sphere with the lowest gloss level, chosen to minimize specular highlights, because such highlights carry little information about the painting style. We then align it with its corresponding rendered sphere. We compute s by dividing the painted image by the rendered one in pixel space, applying constants and scaling factors to ensure numerical stability (Fig. 2). This isolated style representation is then applied to the rendered photorealistic spheres with different gloss levels (rendered with variations of the roughness r parameter of the *Disney’s Principled BSDF* [74]) and used as the style reference for StyLit [72]. Each rendered sphere is produced with a known roughness value, providing an explicit gloss-level label for every sample in the dataset. This yields stylized results of a given geometry g with more controlled strokes than the original samples (Fig. 3). The final dataset results as the combination of three styles

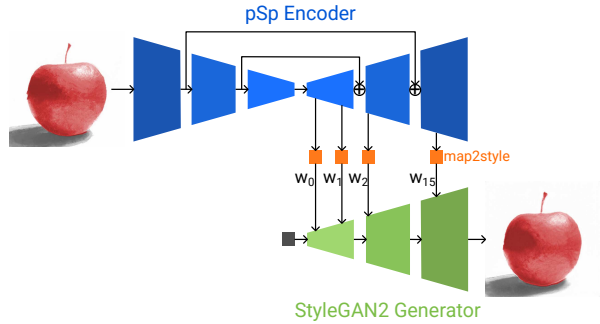


Figure 4: Diagram of the architecture composed by the pSp encoder that constructs a layer-wise latent space through *map2style* layers, and the StyleGAN2 generator, which synthesizes images conditioned on these layer-wise latent representations.

(charcoal, ink pen, and oil painting, which we believe are representative of painting styles), 20 geometries of varied complexity, four illuminations, seven gloss levels, and six colors, resulting in a dataset of 10,080 samples. These generative factors will be used later for evaluating the performance of the model trained without supervision. Representative samples of such dataset can be found in the supplementary material (Sec. S1). The code used in this dataset generation pipeline will be made publicly available to enable reproducibility.

3.3. Architecture

The architecture (Fig. 4) is divided into two modules, trained separately: a StyleGAN2 generator, and a pSp encoder. The generator learns to produce images resembling those of the training dataset (Sec. 3.2), through the traditional adversarial *min–max* optimization of a generator and discriminator, where the latent space W emerges. It also incorporates *path length regularization*, introduced in StyleGAN2, to encourage smoothness in the latent space. Keeping the resulting generator frozen, a pSp encoder is trained for image reconstruction, creating a layer-wise latent space $W+$ where images can be projected in a single forward pass. Its loss function $\mathcal{L}(x) = \lambda_1 \mathcal{L}_2(x) + \lambda_2 \mathcal{L}_{LPIPS}(x) + \lambda_3 \mathcal{L}_{reg}(x)$, as proposed by Richardson et al. [60], encourages both disentanglement and reconstruction accuracy in the extended latent space, properties that are essential to our task. By training both modules in an unsupervised fashion, we do not impose any predefined factors or ordering to be learned in the latent space; instead, these representations are organically learned during the optimization process, using only images as input. For further implementation details, please refer to the supplementary material (Sec. S2.1).

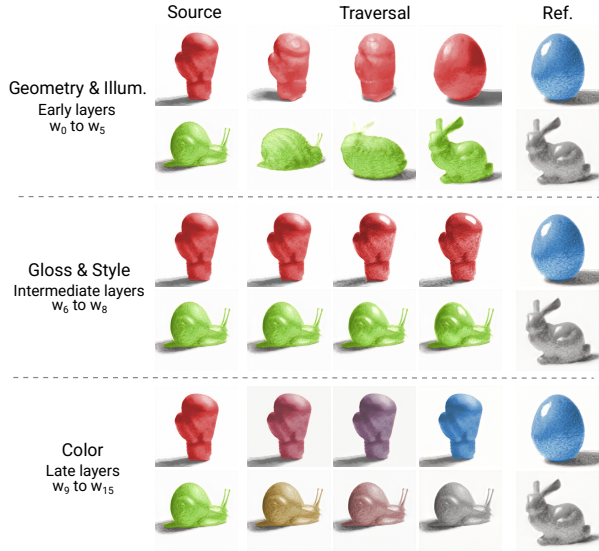


Figure 5: Traversals at different depths of the latent space produce interpretable changes in appearance. Starting from the embeddings of a source image (left), moving along early, intermediate, and late layers respectively induces variations in geometry and illumination, gloss and style, or color.

4. Analysis of the Model

This section presents a comprehensive evaluation of the trained generative pipeline (Sec. 3.3). We begin by assessing its reconstruction ability, by projecting an input sample into W^+ and feeding the resulting embedding to the generator, in order to evaluate potential information loss within the pipeline (Sec. 4.1). Next, we analyze key properties of the learned latent space, including continuity, traversability, disentanglement, and informativeness (Sec. 4.2, Sec. 4.3, and Sec. 4.4). Finally, we run an ablation study on the number of styles handled by the network (Sec. 4.5), studying the robustness of the method when scaling the complexity of the dataset. Additional analysis regarding the internal organization of the latent space and further visualizations can be found in the supplementary material (Sec. S4.3).

4.1. Reconstruction Capabilities of the Pipeline

High reconstruction quality is an important prerequisite for obtaining a meaningful latent space. Without it, any apparent disentanglement might reflect learned noise rather than true factor separation. To verify this, we evaluate whether generative features can propagate from the input image, encoded by pSp , through the StyleGAN2 generator. Our pipeline is able to (i) accurately reconstruct general samples and (ii) closely reproduce the ground-truth gloss traversal (visual results of

various reconstructions are available in the supplementary material, Sec. S3). We also quantitatively evaluate the reconstruction capabilities of the pipeline by computing the metrics of MSE, MAE, PSNR, and SSIM between the reference and reconstructions, obtaining values of 0.003, 0.027, 25.51, and 0.801 respectively.

4.2. Internal Organization of the Latent Space

When analyzing the structure of W^+ , we observed that information is hierarchically distributed across different layers of the space. We hypothesize that this organization arises from the specific information required by the StyleGAN generator at each stage of the synthesis process. As observed in Fig. 5, *early layers* ($w_{0..5}$) primarily encode global scene attributes, such as geometry and illumination. The *middle layers* ($w_{6..8}$) capture finer properties of material appearance, including gloss level and painting style. Finally, the *late layers* ($w_{9..15}$) determine surface-level attributes such as color. Notably, we can observe a clear disentanglement among these factors, which enables predictable manipulations when traversing the latent space.

To quantify how different latent factors are encoded in the network, we exploit the explicit labels available from our dataset generation (gloss level, geometry, style, color, and illumination) and examine how this information is distributed across the 16 layers of the StyleGAN W^+ latent space (each being 512-dimensional). For each layer, we compute a de-biased conditional mutual information [75, 76] between the layer’s embedding X and a target factor Y (e.g., gloss), while conditioning on the remaining factors Z (e.g., geometry or style). This measure subtracts the expected mutual information obtained when the labels Y are randomly permuted, thereby correcting for spurious dependencies caused by correlations among factors:

$$\text{Corr_MI}(X; Y|Z) = I(X; Y|Z) - \mathbb{E}_{\text{perm}}[I(X; Y_{\text{perm}}|Z)],$$

where $I(X; Y|Z) = H(Y|Z) - H(Y|X, Z)$.

Here, $I(X; Y|Z)$ is the conditional mutual information, and H denotes entropy. \mathbb{E}_{perm} represents the average mutual information arising from noise (estimated by permuting the labels), and subtracting it from the estimated conditional mutual information I provides the corrected value Corr_MI . Results of this quantitative analysis are coherent with those qualitative in Fig. 5, revealing that *geometry* and *illumination* are captured in layers 0 to 5, *gloss* is captured in layer 6, *style* is captured in layer 8, and *color* is captured in layers 9 to 15. A complete visualization of the information distribution

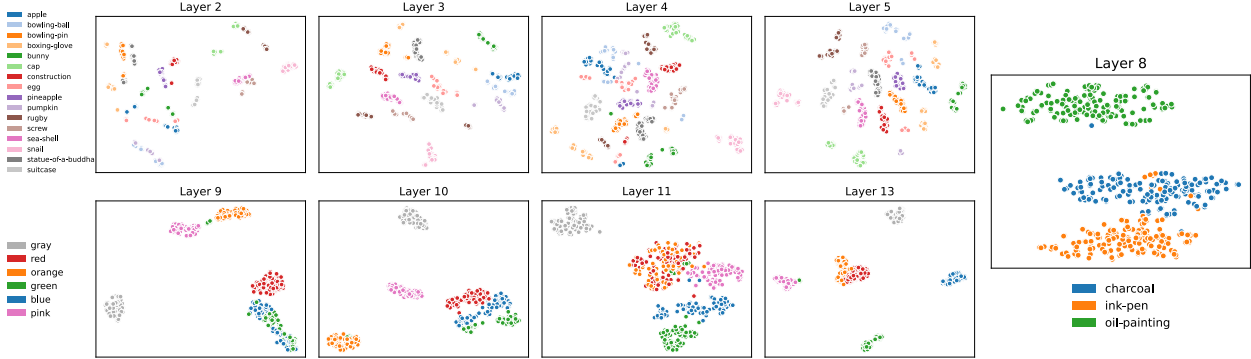


Figure 6: Representative 2D t-SNE visualizations illustrating the internal separation of samples within each label. **Top:** early layers colored by *geometry* labels. **Bottom:** late layers colored by *color* labels. **Right:** Layer 8 colored by *style* layers.

can be found in the supplementary material (Sec. S4.2), together with an additional analysis on the image formation process by inspecting the intermediate representations used by the generator (supplementary material, Sec. S4.3).

These results provide a clear, layer-wise mapping of how different appearance factors are organized inside the generator, offering an interpretable link between the latent architecture and the resulting visual attributes.

4.3. Embedding of Categorical Factors

After confirming that generative factors are hierarchically distributed across layers, we next examine the internal structure of individual layers to assess intra-class disentanglement and information organization. For categorical factors (i.e., geometry, illumination, color, and style), we perform layer-wise t-SNE [77] projections of the 512-dimensional embeddings into a two-dimensional space for visualization, with points colored according to their corresponding labels. This unsupervised approach allows to evaluate not only whether a given layer encodes a particular factor, but also whether its internal representations are organized according to class labels. As illustrated in Fig. 6, each layer exhibits internal clusters corresponding to different class instances. Notably, Layer 8 (Fig. 6, right) achieves a clear separation of styles into three well-defined clusters corresponding with the three input styles. Complete t-SNE visualizations per layer and label can be found in the supplementary material (Sec. S4.1).

4.4. Embedding of Gloss

In this section, we examine how Layer 6 embeddings relate to the gloss labels in our dataset. Unlike the categorical factors studied in Sec. 4.3, gloss represents an ordinal variable, which makes the unsupervised t-SNE

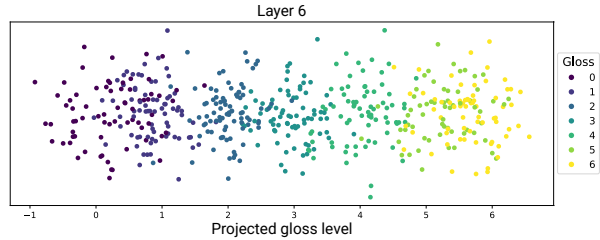


Figure 7: Projection of samples onto a one-dimensional space learned with a linear ridge regression model. Points are jittered along the vertical axis for visibility and colored according to their ground-truth *gloss* labels. Each point is projected using a model that was trained without that sample (cross-validation).

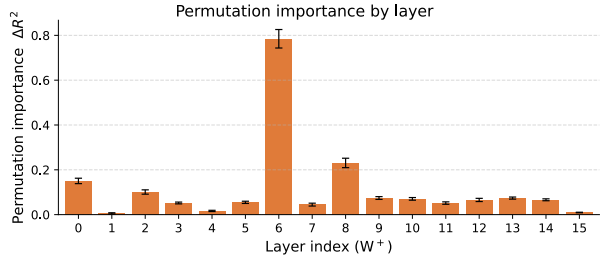


Figure 8: Uniqueness of gloss information per layer, measured by ΔR^2 variations when predicting gloss labels without layer i . More details in the text.

method unsuitable: t-SNE is designed to preserve local neighborhood relationships but does not maintain the global ordering needed to assess gradual changes in gloss. We therefore employ alternative analyses to test whether the internal representation in Layer 6 reflects the expected progression of gloss levels.

As a first step, we apply supervised Ridge regression to predict gloss from the Layer 6 embeddings. Using cross-validation, we train five separate models on different subsets of the training data and, for each model,

project the held-out validation samples onto the resulting one-dimensional regression axis (samples are scattered uniformly along the y -axis in the plot for clarity). Each validation sample is always excluded from the training set of its corresponding model. The results, shown in Fig. 7, reveal a well-defined linear trend with respect to gloss. Quantitatively, the resulting projections achieve a prediction MSE of 0.1224 ± 0.0229 against the ground truth and a Spearman correlation of 0.97, confirming a strong monotonic relationship between the learned representation and the ground-truth gloss levels.

We next assess the unique contribution of each layer to the prediction of gloss. To this end, we first train a supervised linear model on all layers which learns to predict gloss labels. At test time, we evaluate the performance drop (by means of R^2 variation) when the embeddings of a given layer i are made uninformative by randomly permuting them. A substantial decrease in performance when w_i is permuted indicates that Layer i contains unique information about gloss that cannot be compensated for by other layers, meaning that this layer is explanatory of gloss. Consistent with previous visualizations, Fig. 8 shows that Layer 6 encodes the highest amount of unique gloss-related information.

Altogether, these results reveal a clear and interpretable encoding of gloss within the latent space, showing that this perceptual attribute can emerge spontaneously in an unsupervised model even when trained on painterly depictions with wide variation in artistic styles.

4.5. Ablation on the Number of Styles

In this section, we analyze the effect of varying the number of styles included in the dataset. We quantitatively assess the *latent space compactness* as a proxy for disentanglement, utilizing the regularization metric (Reg) proposed by Richardson et al. [60].

We also compute the Perceptual Path Length (PPL) which, since its introduction in the StyleGAN paper [61], has been widely used to evaluate the *smoothness and continuity* of latent spaces.

Tab. 1 shows the result of training four different models with increasing number of styles. We observe a trend where smoothness and continuity of the latent spaces (measured by PPL) remains steady despite variations in the number of styles, showing that the continuity property of the GAN-based pipeline is not affected by complexity increments in the dataset. On the other hand, we see how an increasing complexity in the dataset (here represented as a larger number of styles) naturally leads to a gradual and controlled decrease of the latent space

Table 1: Quantitative results for the ablation study on the number of styles. Reported metrics represent compactness (Reg , lower is better), and smoothness (PPL , lower is better) of the latent spaces.

#Styles	2	3	4	5
Reg ↓	11.13	18.40	21.68	22.13
PPL ↓	54.32	54.03	60.22	55.20

compactness (higher Reg values), which needs to account for the increased amount of information. This shows how the setup used in the work can be expanded to additional styles while keeping the *disentanglement* and *compactness* properties.

For additional details on the metrics used in this section, please refer to the supplementary material (Sec. S5).

Taken together, these analyses reveal a rich and interpretable organization of gloss and style within the latent space, showing that complex appearance cues can emerge without supervision. This understanding provides a solid foundation for the controlled image-synthesis application explored in the next section.

5. Application: Style- and Gloss-guided Diffusion Pipeline

We propose a diffusion pipeline that enables intuitive and controllable stylization of a reference image by leveraging the style- and gloss-aware latent space identified in Sec. 4. To avoid the costly and time-intensive process of training diffusion models from scratch, recent research has explored combining the strengths of GANs (e.g. disentanglement, continuity, and latent space interpretability) with those of diffusion models (e.g. robustness, generalizability, and image quality) [18, 19]. A common strategy involves the use of lightweight adapters [78], which provide a balance between efficient training and effective conditioning by reusing the strong priors of pretrained models while incorporating novel cues.

In our proposed pipeline, the adapter conditions generation on *gloss* and *style* features by leveraging the information encoded in the intermediate $W+$ embeddings (W_I^+); Our previous experiments have shown that these embeddings are disentangled and highly informative of these two factors (Sec. 4.2), making them well-suited for fine-grained control. The text prompt conditions complementary factors such as *geometry*, *illumination*, and *color*. This design allows the model to exploit the pretrained text encoder’s prior knowledge, thereby generalizing to novel geometries or colors not

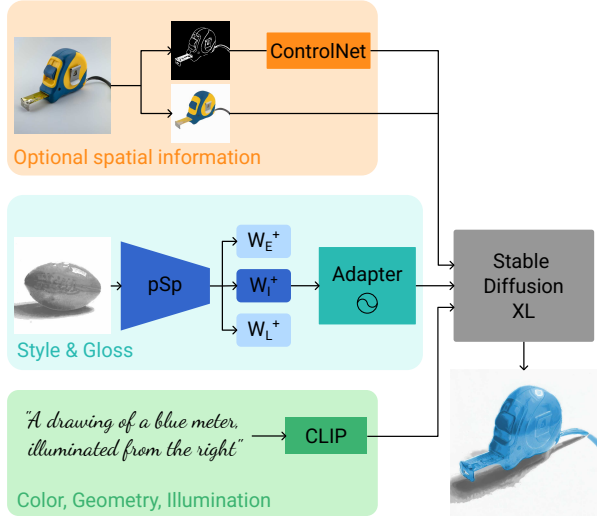


Figure 9: **Diagram of the proposed diffusion-based pipeline.** It can handle up to three inputs: (i) a text prompt defining the color, geometry, and illumination, (ii) a style and gloss reference image that uses the intermediate layers of the latent space created in previous sections, and (iii) an optional image to guide spatial information of geometry and albedo.

observed during training of the adapter. To further enhance geometric control, we propose to integrate a pre-trained ControlNet conditioned on Canny edges [12]. Finally, the user may optionally include an albedo map to specify the base albedo of the shape, providing finer-grained control over color. We base the implementation of our custom adapter on that of *W+ Adapter* [18], using Stable Diffusion XL 1.0 as backbone of the diffusion pipeline, and use as loss function the accuracy of the model when predicting the injected noise, as originally proposed by Rombach et al. [79]. We compare the performance of our model against state-of-the-art approaches, including (i) general-purpose text-to-image (T2I) models, (ii) style transfer methods, and (iii) Artist-Inator [32], a recent diffusion-based non-photorealistic stylization framework that is the closest related work to ours. An overview of the designed pipeline is shown in Fig. 9. Additional implementation details can be found in the supplementary material (Sec. S2.2).

5.1. Evaluation of Results

This section presents qualitative and quantitative results of the proposed pipeline, including: (i) an evaluation of its different conditioning strategies, (ii) a comparison with prior work, and (iii) an analysis of the granularity when defining perceptual attributes such as gloss.

Conditioning via Text Prompt. The minimal conditioning setup of the pipeline requires an input image for style and gloss guidance, and a text prompt for color, geometry, and illumination guidance. Current implementation allows defining one of the four illuminations used in the training dataset (Sec. 3.2) via text prompt (e.g., *illuminated from the right*). Definition of color and geometry through text prompt can be made via free text, and results ultimately depend on the expressivity and accuracy of text embeddings, obtained with the pretrained text encoder used (in our case, CLIP [80]). Although versatile, defining geometry solely through text introduces variability proportional to the ambiguity of the described instance (e.g. the shape of *Yoda* is more specific than that of *toy*). A Figure illustrating several examples generated under this text-based conditioning can be visualized in the supplementary material (Sec. S6). Results demonstrate that targeted modifications can be achieved intuitively by altering only specific parts of the text or image prompt, while leaving the other factors unchanged.

Conditioning with Additional Spatial Information. As illustrated in the pipeline architecture (Fig. 9), additional spatial information can be introduced to control both shape and color. Shape is specified using a Canny edge map, which is then fed to a ControlNet [12], while color is defined through an albedo map computed automatically with Marigold [81]. The albedo map is applied during the late stage of the diffusion process to adjust the latent representations at inference time. As shown in Fig. 10, this strategy enables precise control over the output geometry, effectively supporting style transfer with the learned styles. Additionally, the current configuration enables automatic generalization to diverse geometry representations, including clip-arts.

Comparison with Prior Work. Image synthesis methods have attracted increasing attention due to the unprecedented quality achieved by recent generative models. We evaluate our approach against representative methods from three categories:

- General-purpose text-to-image (T2I) methods, which generate images directly from text prompts (with no *style* reference), and are designed for a broad range of tasks. This category includes the methods of FLUX [82] and GPT Image 1 [83]
- Style transfer architectures, which specialize in transferring a reference style onto a target content image. We evaluate against StyleID [84], DEAD-iff [29], and InstantStyle [85].
- Artist-Inator [32], a gloss-aware stylization

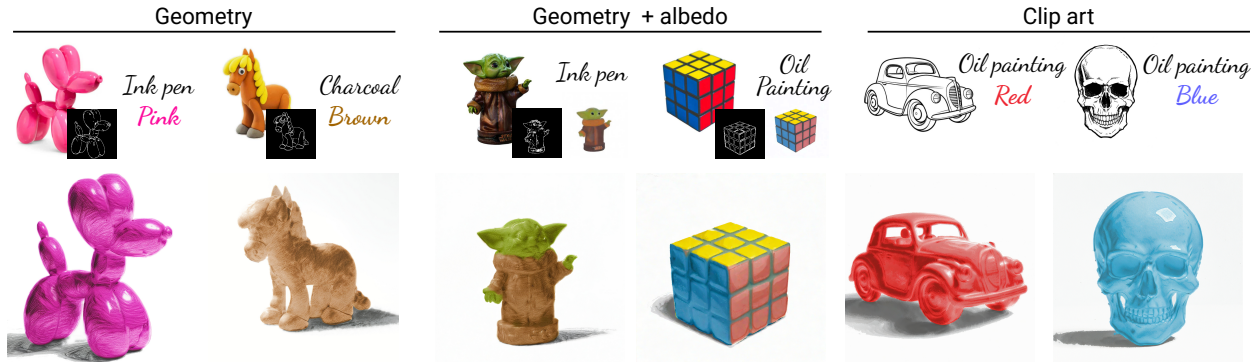


Figure 10: Examples of three input modalities supported by our pipeline. Our method allows different levels of conditioning on geometry and color: color can be specified through a text prompt (left) or through spatial guidance using an albedo map (middle). Geometry is provided as edge or border maps, and by leveraging a ControlNet pretrained on Canny edges the pipeline also generalizes to other geometric representations such as clip-art drawings (right).

method, which represents the closest approach to our work.

All models are guided on geometrical information using the same input image (Fig. 11, first column), and style is defined either via an image input (Fig. 11, second column), or via a textual description, depending on the method’s requirements. The remaining factors of *style*, *gloss*, *color*, and *illumination* are defined via text prompt for T2I methods and Artist-Inator, while style transfer models use an additional reference image. Results in Fig. 11 reveal a trend in which general-purpose methods produce the most visually appealing outputs, at the cost of a lower adherence to the specific style. In contrast, style transfer approaches show reduced performance, which we attribute to domain shift: some of them rely on general-purpose image encoders that perform well with in-the-wild images, but are less effective with our non-photorealistic depictions of isolated objects on a white background. Finally, our method achieves strong adherence to both the reference style and gloss cues, while maintaining an adequate image quality. Further details regarding the execution of each of the aforementioned methods and the design of the user study are provided in the supplementary material (Sec. S7).

User Study. We conducted a user study to further validate the performance of our model. A total of 22 participants (mean age = 28.9 years; 7 female) took part in the study, evaluating which alternative achieved better style transfer across 12 experimental setups. We used a subset of the methods composed by DEADiff, InstantStyle, Artist-Inator, and ours, and computed the following metrics:

- Preference, which reflects with what percentage

Table 2: Results of the user study comparing our method with other style transfer approaches. We report the preference rate of our method over each alternative (Preference) and the overall Rank Product across all methods. Higher Preference and lower Rank Product indicate better performance.

Method	Preference ↑	Rank Product ↓
DEADiff	97.73%	3.435
InstantStyle	83.71%	2.142
Artist-Inator	93.18%	2.778
<i>Ours</i>	—	1.172

our model was preferred over a certain alternative.

- Rank Product (RP), which reflects the overall user preference across all questions, and is computed as $RP(g) = (\prod_{k=1}^K r_{g,k})^{\frac{1}{K}}$, where $r_{g,k}$ represents the average ranking achieved by model g in question k , and $K = 12$.

The results of the user study (Tab. 2) show that participants consistently preferred our method over the presented alternatives, which is coherent with prior qualitative analysis.

Continuous Representation of Gloss A central strength of our approach lies in the precise control it offers over gloss. Leveraging the good properties of our $W+$ space regarding continuity of the gloss attribute (Sec. 4.4), we evaluate to what extent this property is preserved by the trained adapter and compare its performance with prior approaches. As shown in Fig. 12, our model achieves the most faithful and continuous traversal of the gloss dimension, progressively adjusting highlights and specularities to increase perceived gloss while leaving other appearance factors unchanged. Among

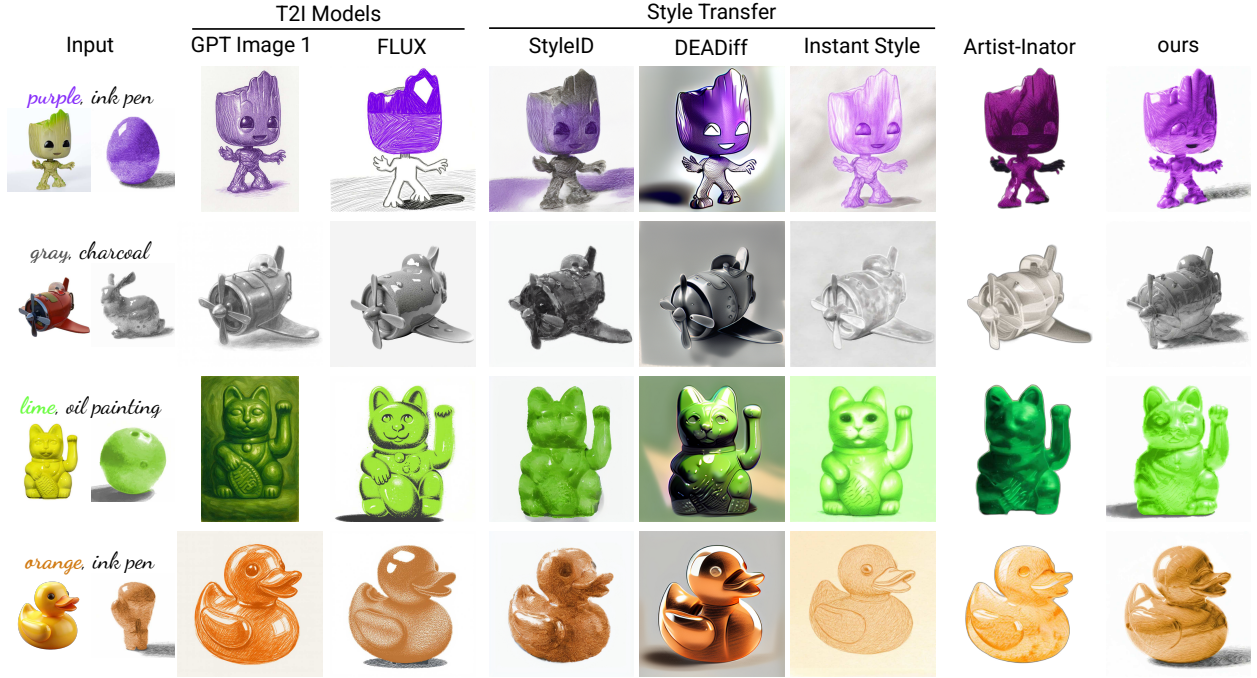


Figure 11: **Qualitative comparison with state-of-the-art models.** General-purpose T2I models produce visually striking images but often deviate from the target style and geometry. GPT Image 1 can often approximate the reference style, but its outputs offer only limited fine-grained control and may vary across prompts, making precise manipulation more challenging than with our method (Fig. 12). Style-transfer methods better respect the reference style but tend to generate less compelling or less stable outputs. Our method achieves visually appealing results while maintaining high fidelity to both the reference geometry and the intended painterly style.

competing approaches, Artist-Inator [32] generally follows the gloss instruction, particularly at the extremes, but fails to produce a smooth progression. GPT Image 1 [83] again delivers visually attractive outputs, but this comes at the cost of limited controllability over gloss.

6. Discussion and Limitations

We presented a comprehensive analysis of how perceptual factors naturally organize within a hierarchical GAN-based architecture. Focusing on non-photorealistic imagery, we examined the interdependencies between artistic styles and other perceptual attributes, with a particular emphasis on gloss. Our analysis revealed a latent space that disentangles style from gloss, showing that a generative model can separate such factors without relying on explicit labels. Building on this representation, we trained a lightweight adapter that enables the generation of non-photorealistic images of arbitrary objects with fine-grained control over style and gloss, while supporting flexible conditioning of geometry, color, and illumination through text and image references.

While prior analyses of latent spaces focus on understanding emergent perceptual factors [50], they do not demonstrate whether they can be used to effectively control generation. Conversely, prior NPR-oriented generative work (notably Artist-Inator [32]) provides stylization capabilities but does not yield a disentangled representation of perceptual factors and thus cannot offer predictable factor-wise control. Our work bridges these two directions: we introduce a style- and gloss-aware latent space, and show that exploiting this space leads to improved control and better style preservation, as confirmed by our user study. Finally, as discussed in Sec. 5.1, while our method may lack the generative capacity of large-scale general-purpose models such as GPT Image 1, it provides a suitable alternative in scenarios where precise control over generative factors is required. Moreover, the disentangled structure of the latent space enables a higher degree of interpretability by directly inspecting the latent representation driving the generated image, an aspect that remains largely inaccessible in general-purpose models such as GPT Image 1.

Our proposed approach does have certain limitations. First, we restricted the number of styles to three – charcoal, ink pen, and oil painting –, choosing them to

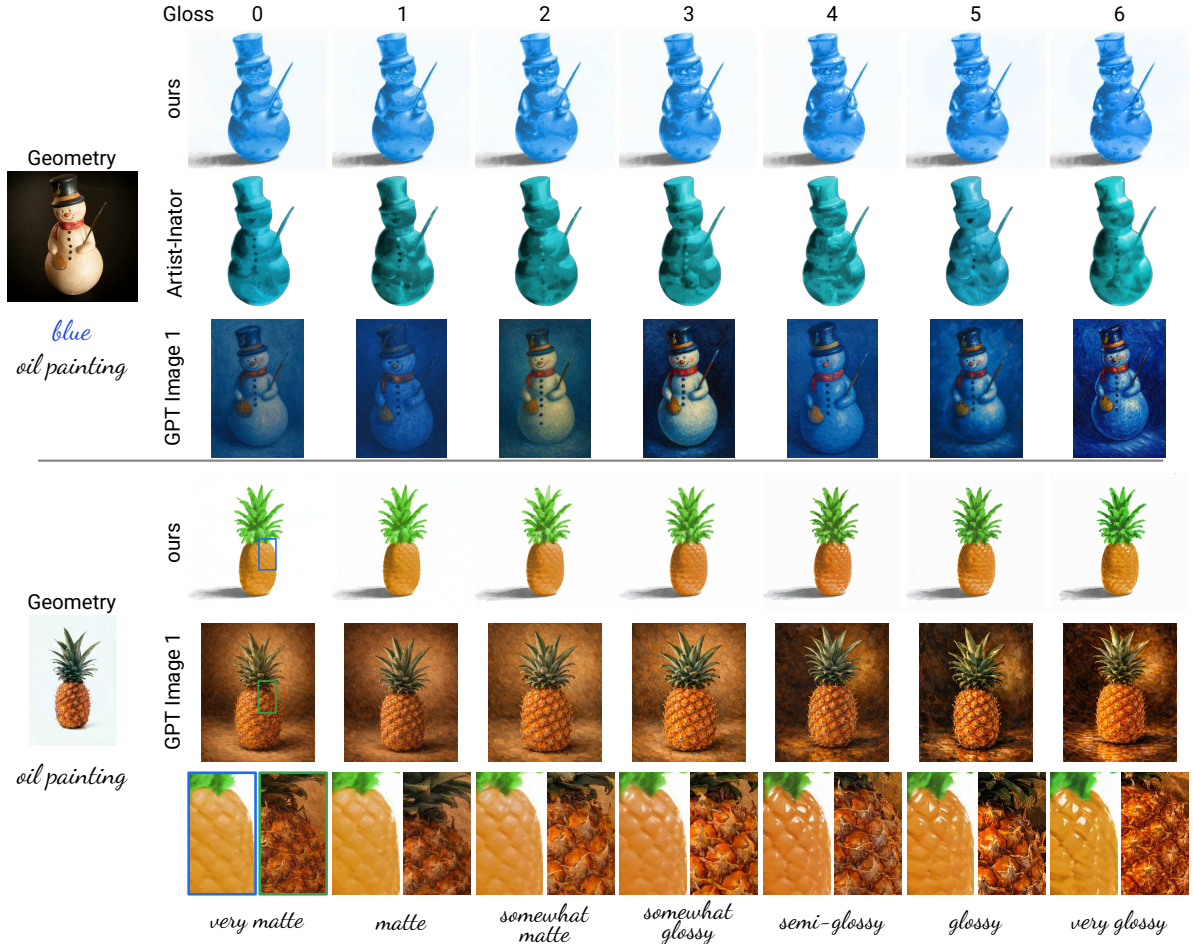


Figure 12: **Comparison of gloss control.** We compare our method with Artist-Inator [32] and GPT Image 1 [83], for two inputs (left-most column). For our method, target gloss level is specified through a slider (shown at the top of the figure), while for both competing methods it is specified through a text prompt (shown at the bottom). In the second example (bottom half) our result is also conditioned on the albedo map estimated from the source, and compared to GPT Image 1 (Artist-Inator only handles monochromatic outputs), including zoomed-in crops of the same region in both methods. Our approach provides a clear and progressive modulation of gloss while keeping geometry and overall style stable. On the other hand, both alternatives exhibit limited ability to generate a smooth and continuous change in gloss; in particular, GPT Image 1 generates overall striking results, but at the cost of struggling to produce consistent gloss gradation.

be representative of a variety of hand-drawn or hand-painted styles. As a result, our model cannot natively generalize to unseen styles such as soft crayon or watercolor; handling these would require explicit training or fine-tuning. Nonetheless, the modular training and analysis framework used here could be easily extended to incorporate additional styles in future work. A second limitation relates to the degree of control over the color: in the current implementation, the albedo map is applied during late stages of the diffusion process; while it works well generally, this strategy can lead to the loss of color information, particularly in fine details. ControlNets [12] are a well-established approach to condition image generation on spatial information (such as

albedo maps). However, to the best of our knowledge, no validated pretrained ControlNet for albedo maps is currently available for Stable Diffusion XL, and this therefore remains future work. Finally, another interesting line for future work would be to combine traversals in our disentangled $W+$ space with those in a more general-purpose space such as CLIP [86, 87], potentially combining their conditioning capabilities.

Recent advances in generative image synthesis have reached unprecedented levels of visual fidelity, to the point that generated images can be indistinguishable from real photographs to the naked eye. However, these capabilities often rely on models with billions of parameters, which significantly hinders the explainability of

their outputs. Interpretability constitutes an important research direction in the study of large-scale generative models, and we hope this work inspires new developments on controllable generative models and their relation to human visual perception, leading to improved content authoring tools. Our trained model, code and dataset will be made public soon.

References

- [1] R. W. Fleming, R. O. Dror, E. H. Adelson, Real-World Illumination and the Perception of Surface Reflectance Properties, *Journal of Vision* 3 (5) (2003) 3. [doi:10.1167/3.5.3](https://doi.org/10.1167/3.5.3).
- [2] R. W. Fleming, Material Perception, *Annual Review of Vision Science* 3 (Volume 3, 2017) (2017) 365–388, publisher: Annual Reviews. [doi:10.1146/annurev-vision-102016-061429](https://doi.org/10.1146/annurev-vision-102016-061429).
- [3] F. Schmidt, M. N. Hebart, A. C. Schmid, R. W. Fleming, Core Dimensions of Human Material Perception, *Proceedings of the National Academy of Sciences* 122 (10) (2025) e2417202122, publisher: Proceedings of the National Academy of Sciences. [doi:10.1073/pnas.2417202122](https://doi.org/10.1073/pnas.2417202122).
- [4] M. Lagunas, A. Serrano, D. Gutierrez, B. Masia, The Joint Role of Geometry and Illumination on Material Recognition, *Journal of Vision* 21 (2) (2021) 2. [doi:10.1167/jov.21.2.2](https://doi.org/10.1167/jov.21.2.2).
- [5] A. Serrano, B. Chen, C. Wang, M. Piovarči, H.-P. Seidel, P. Didyk, K. Myszkowski, The Effect of Shape and Illumination on Material Perception: Model and Applications, *ACM Trans. Graph.* 40 (4) (2021) 125:1–125:16. [doi:10.1145/3450626.3459813](https://doi.org/10.1145/3450626.3459813).
- [6] B. Chen, C. Wang, M. Piovarči, H.-P. Seidel, P. Didyk, K. Myszkowski, A. Serrano, The Effect of Geometry and Illumination on Appearance Perception of Different Material Categories, *The Visual Computer* 37 (12) (2021) 2975–2987. [doi:10.1007/s00371-021-02227-x](https://doi.org/10.1007/s00371-021-02227-x).
- [7] A. C. Chadwick, R. W. Kentridge, The perception of gloss: A review, *Vision Research* 109 (2015) 221–235. [doi:10.1016/j.visres.2014.10.026](https://doi.org/10.1016/j.visres.2014.10.026).
- [8] M. J. P. van Zuijlen, S. C. Pont, M. W. A. Wijntjes, Painterly Depiction of Material Properties, *Journal of Vision* 20 (7) (2020) 7. [doi:10.1167/jov.20.7.7](https://doi.org/10.1167/jov.20.7.7).
- [9] J. Delanoy, A. Serrano, B. Masia, D. Gutierrez, Perception of Material Appearance: A Comparison Between Painted and Rendered Images, *Journal of Vision* 21 (5) (2021) 16. [doi:10.1167/jov.21.5.16](https://doi.org/10.1167/jov.21.5.16).
- [10] Y. Zhao, J. Stumpel, H. de Ridder, M. W. A. Wijntjes, Material Perception Across Different Media—Comparing Perceived Attributes in Oil Paintings and Engravings, *i-Perception* 15 (4) (2024) 20416695241261140, publisher: SAGE Publications. [doi:10.1177/20416695241261140](https://doi.org/10.1177/20416695241261140).
- [11] R. Po, W. Yifan, V. Golyanik, K. Aberman, J. T. Barron, A. Bermano, E. Chan, T. Dekel, A. Holynski, A. Kanazawa, C. Liu, L. Liu, B. Mildenhall, M. Nießner, B. Ommer, C. Theobalt, P. Wonka, G. Wetzstein, State of the Art on Diffusion Models for Visual Computing, *Computer Graphics Forum* 43 (2) (2024) e15063. [doi:10.1111/cgf.15063](https://doi.org/10.1111/cgf.15063).
- [12] L. Zhang, A. Rao, M. Agrawala, Adding Conditional Control to Text-to-Image Diffusion Models, in: 2023 IEEE/CVF International Conference on Computer Vision (ICCV), 2023, pp. 3813–3824, ISSN: 2380-7504. [doi:10.1109/ICCV51070.2023.00355](https://doi.org/10.1109/ICCV51070.2023.00355).
- [13] S. F. Bhat, N. Mitra, P. Wonka, LOOSE-ONTROL: Lifting ControlNet for Generalized Depth Conditioning, in: ACM SIGGRAPH 2024 Conference Papers, SIGGRAPH '24, Association for Computing Machinery, New York, NY, USA, 2024, pp. 1–11. [doi:10.1145/3641519.3657525](https://doi.org/10.1145/3641519.3657525).
- [14] M. Li, T. Yang, H. Kuang, J. Wu, Z. Wang, X. Xiao, C. Chen, ControlNet++: Improving Conditional Controls with Efficient Consistency Feedback, in: Computer Vision – ECCV 2024, Springer Nature Switzerland, Cham, 2025, pp. 129–147. [doi:10.1007/978-3-031-72667-5_8](https://doi.org/10.1007/978-3-031-72667-5_8).
- [15] E. Bernal-Berdun, A. Serrano, B. Masia, M. Gadelha, Y. Hold-Geoffroy, X. Sun, D. Gutierrez, PreciseCam: Precise Camera Control for Text-to-Image Generation, in: 2025 IEEE/CVF Conference on Computer Vision and Pattern Recognition (CVPR), 2025, pp. 2724–2733, ISSN: 2575-7075. [doi:10.1109/CVPR52734.2025.00260](https://doi.org/10.1109/CVPR52734.2025.00260).

[16] E. Härkönen, A. Hertzmann, J. Lehtinen, S. Paris, GANSpace: Discovering Interpretable GAN Controls, in: Proceedings of the 34th International Conference on Neural Information Processing Systems, NIPS '20, Curran Associates Inc., Red Hook, NY, USA, 2020, pp. 9841–9850. [doi:10.48550/arXiv.2004.02546](https://doi.org/10.48550/arXiv.2004.02546).

[17] D. Bau, J.-Y. Zhu, H. Strobelt, B. Zhou, J. B. Tenenbaum, W. T. Freeman, A. Torralba, GAN Dissection: Visualizing and Understanding Generative Adversarial Networks, in: International Conference on Learning Representations (ICLR), 2019. [doi:10.48550/arXiv.1811.10597](https://doi.org/10.48550/arXiv.1811.10597).

[18] X. Li, X. Hou, C. C. Loy, When StyleGAN Meets Stable Diffusion: a W+ Adapter for Personalized Image Generation, in: 2024 IEEE/CVF Conference on Computer Vision and Pattern Recognition (CVPR), 2024, pp. 2187–2196, iSSN: 2575-7075. [doi:10.1109/CVPR52733.2024.00213](https://doi.org/10.1109/CVPR52733.2024.00213).

[19] R. Gandikota, J. Materzyńska, T. Zhou, A. Torralba, D. Bau, Concept Sliders: LoRA Adapters for Precise Control in Diffusion Models, in: Computer Vision – ECCV 2024, Springer Nature Switzerland, Cham, 2025, pp. 172–188. [doi:10.1007/978-3-031-73661-2_10](https://doi.org/10.1007/978-3-031-73661-2_10).

[20] S. Jimenez-Navarro, J. Guerrero-Viu, B. Masia, A Controllable Appearance Representation for Flexible Transfer and Editing, in: Eurographics Symposium on Rendering, The Eurographics Association, 2025. [doi:10.2312/sr.20251187](https://doi.org/10.2312/sr.20251187).

[21] P. Haeberli, Paint by Numbers: Abstract Image Representations, SIGGRAPH Comput. Graph. 24 (4) (1990) 207–214. [doi:10.1145/97880.97902](https://doi.org/10.1145/97880.97902).

[22] A. Hertzmann, Painterly Rendering With Curved Brush Strokes of Multiple Sizes, in: Proceedings of the 25th annual conference on Computer graphics and interactive techniques, SIGGRAPH '98, Association for Computing Machinery, New York, NY, USA, 1998, pp. 453–460. [doi:10.1145/280814.280951](https://doi.org/10.1145/280814.280951).

[23] A. Hertzmann, A Survey of Stroke-Based Rendering, IEEE Computer Graphics and Applications 23 (4) (2003) 70–81. [doi:10.1109/MCG.2003.1210867](https://doi.org/10.1109/MCG.2003.1210867).

[24] L. A. Gatys, A. S. Ecker, M. Bethge, A Neural Algorithm of Artistic Style, published as Vision Sciences Society Annual Meeting Abstract (Sep. 2015). [doi:10.48550/arXiv.1508.06576](https://doi.org/10.48550/arXiv.1508.06576).

[25] Y. Jing, Y. Liu, Y. Yang, Z. Feng, Y. Yu, D. Tao, M. Song, Stroke Controllable Fast Style Transfer with Adaptive Receptive Fields, in: Computer Vision – ECCV 2018, Springer International Publishing, Cham, 2018, pp. 244–260. [doi:10.1007/978-3-030-01261-8_15](https://doi.org/10.1007/978-3-030-01261-8_15).

[26] K. Simonyan, A. Zisserman, Very deep convolutional networks for large-scale image recognition, in: International Conference on Learning Representations (ICLR), 2015. [doi:10.48550/arXiv.1409.1556](https://doi.org/10.48550/arXiv.1409.1556).

[27] R. Abdal, Y. Qin, P. Wonka, Image2StyleGAN: How to Embed Images Into the StyleGAN Latent Space?, in: 2019 IEEE/CVF International Conference on Computer Vision (ICCV), 2019, pp. 4431–4440, iSSN: 2380-7504. [doi:10.1109/ICCV.2019.00453](https://doi.org/10.1109/ICCV.2019.00453).

[28] H. Tang, H. Liu, D. Xu, P. H. S. Torr, N. Sebe, AttentionGAN: Unpaired Image-to-Image Translation Using Attention-Guided Generative Adversarial Networks, IEEE Transactions on Neural Networks and Learning Systems 34 (4) (2023) 1972–1987. [doi:10.1109/TNNLS.2021.3105725](https://doi.org/10.1109/TNNLS.2021.3105725).

[29] T. Qi, S. Fang, Y. Wu, H. Xie, J. Liu, L. Chen, Q. He, Y. Zhang, DEADiff: An Efficient Stylization Diffusion Model with Disentangled Representations, in: 2024 IEEE/CVF Conference on Computer Vision and Pattern Recognition (CVPR), 2024, pp. 8693–8702, iSSN: 2575-7075. [doi:10.1109/CVPR52733.2024.00830](https://doi.org/10.1109/CVPR52733.2024.00830).

[30] Z. Wang, X. Wang, L. Xie, Z. Qi, Y. Shan, W. Wang, P. Luo, StyleAdapter: A Unified Stylized Image Generation Model, International Journal of Computer Vision 133 (4) (2025) 1894–1911. [doi:10.1007/s11263-024-02253-x](https://doi.org/10.1007/s11263-024-02253-x).

[31] Q. Wang, H.-N. Dai, J. Yang, C. Guo, P. Childs, M. Kleinsmann, Y. Guo, P. Wang, Learning-based Artificial Intelligence Artwork: Methodology Taxonomy and Quality Evaluation, ACM Comput. Surv. 57 (3) (2024) 71:1–71:37. [doi:10.1145/3698105](https://doi.org/10.1145/3698105).

[32] J. D. Subias, S. Daniel-Soriano, D. Gutierrez, A. Serrano, Artist-Inator: Text-based, Gloss-aware Non-photorealistic Stylization, Computer

Graphics Forum 44 (4) (2025) e70182. [doi:10.1111/cgf.70182](https://doi.org/10.1111/cgf.70182).

[33] P. Cavanagh, The Artist as Neuroscientist, *Nature* 434 (7031) (2005) 301–307, publisher: Nature Publishing Group. [doi:10.1038/434301a](https://doi.org/10.1038/434301a).

[34] A. Bousseau, J. P. O’shea, F. Durand, R. Ramamoorthi, M. Agrawala, Gloss Perception in Painterly and Cartoon Rendering, *ACM Trans. Graph.* 32 (2) (2013) 18:1–18:13. [doi:10.1145/2451236.2451244](https://doi.org/10.1145/2451236.2451244).

[35] B. Sayim, P. Cavanagh, The Art of Transparency, *i-Perception* 2 (7) (2011) 679–696, publisher: SAGE Publications. [doi:10.1068/i0459aap](https://doi.org/10.1068/i0459aap).

[36] M. W. A. Wijntjes, C. Spoiala, H. d. Ridder, Thurstonian Scaling and the Perception of Painterly Translucency, *Art & Perception* 8 (3-4) (2020) 363–386, publisher: Brill. [doi:10.1163/22134913-bja10021](https://doi.org/10.1163/22134913-bja10021).

[37] F. Di Cicco, M. J. P. van Zuijlen, M. W. A. Wijntjes, S. C. Pont, Soft Like Velvet and Shiny Like Satin: Perceptual Material Signatures of Fabrics Depicted in 17th Century Paintings, *Journal of Vision* 21 (5) (2021) 10. [doi:10.1167/jov.21.5.10](https://doi.org/10.1167/jov.21.5.10).

[38] J. A. Thomas, Fabric and Dress in Bronzino’s Portrait of Eleanor of Toledo and Son Giovanni, *Zeitschrift für Kunstgeschichte* 57 (2) (1994) 262–267, publisher: Deutscher Kunstverlag GmbH Munchen Berlin. [doi:10.2307/1482735](https://doi.org/10.2307/1482735).

[39] J. Chao, P. Cavanagh, D. Wang, Reflections in Art, *Spatial Vision* 21 (3-5) (2008) 261–270, publisher: Brill. [doi:10.1163/156856808784532581](https://doi.org/10.1163/156856808784532581).

[40] F. Di Cicco, M. W. A. Wijntjes, S. C. Pont, Understanding Gloss Perception Through the Lens of Art: Combining Perception, Image Analysis, and Painting Recipes of 17th Century Painted Grapes, *Journal of Vision* 19 (3) (2019) 7. [doi:10.1167/19.3.7](https://doi.org/10.1167/19.3.7).

[41] Y. Zhao, J. Stumpel, H. de Ridder, M. W. A. Wijntjes, Zooming in on Style: Exploring Style Perception Using Details of Paintings, *Journal of Vision* 23 (6) (2023) 2. [doi:10.1167/jov.23.6.2](https://doi.org/10.1167/jov.23.6.2).

[42] A. Elgammal, B. Liu, D. Kim, M. Elhoseiny, M. Mazzone, The Shape of Art History in the Eyes of the Machine, *Proceedings of the AAAI Conference on Artificial Intelligence* 32 (1) (Apr. 2018). [doi:10.1609/aaai.v32i1.11894](https://doi.org/10.1609/aaai.v32i1.11894).

[43] R. W. Fleming, C. Wiebel, K. Gegenfurtner, Perceptual Qualities and Material Classes, *Journal of Vision* 13 (8) (2013) 9. [doi:10.1167/13.8.9](https://doi.org/10.1167/13.8.9).

[44] R. W. Fleming, Visual Perception of Materials and Their Properties, *Vision Research* 94 (2014) 62–75. [doi:10.1016/j.visres.2013.11.004](https://doi.org/10.1016/j.visres.2013.11.004).

[45] C. Zhuang, S. Yan, A. Nayebi, M. Schrimpf, M. C. Frank, J. J. DiCarlo, D. L. K. Yamins, Unsupervised Neural Network Models of the Ventral Visual Stream, *Proceedings of the National Academy of Sciences* 118 (3) (2021) e2014196118, publisher: Proceedings of the National Academy of Sciences. [doi:10.1073/pnas.2014196118](https://doi.org/10.1073/pnas.2014196118).

[46] J. Raugel, M. Szafraniec, H. V. Vo, C. Couprie, P. Labatut, P. Bojanowski, V. Wyart, J.-R. King, Disentangling the Factors of Convergence between Brains and Computer Vision Models, *arXiv Preprint arXiv:2508.18226* (Aug. 2025). [doi:10.48550/arXiv.2508.18226](https://doi.org/10.48550/arXiv.2508.18226).

[47] K. R. Storrs, B. L. Anderson, R. W. Fleming, Unsupervised Learning Predicts Human Perception and Misperception of Gloss, *Nature Human Behaviour* 5 (10) (2021) 1402–1417, publisher: Nature Publishing Group. [doi:10.1038/s41562-021-01097-6](https://doi.org/10.1038/s41562-021-01097-6).

[48] K. E. Prokott, H. Tamura, R. W. Fleming, Gloss Perception: Searching for a Deep Neural Network That Behaves Like Humans, *Journal of Vision* 21 (12) (2021) 14. [doi:10.1167/jov.21.12.14](https://doi.org/10.1167/jov.21.12.14).

[49] T. Morimoto, A. Akbarinia, K. R. Storrs, J. R. Cheeseman, H. E. Smithson, K. R. Gegenfurtner, R. W. Fleming, Human Gloss Perception Reproduced by Tiny Neural Networks, iSSN: 2692-8205 Pages: 2025.05.09.653112 Section: New Results (Nov. 2025). [doi:10.1101/2025.05.09.653112](https://doi.org/10.1101/2025.05.09.653112).

[50] C. Liao, M. Sawayama, B. Xiao, Unsupervised Learning Reveals Interpretable Latent Representations for Translucency Perception, *PLOS Computational Biology* 19 (2) (2023) e1010878, publisher: Public Library of Science. [doi:10.1371/journal.pcbi.1010878](https://doi.org/10.1371/journal.pcbi.1010878).

[51] J. J. R. v. Assen, S. Nishida, R. W. Fleming, Visual Perception of Liquids: Insights From Deep Neural Networks, *PLOS Computational Biology* 16 (8) (2020) e1008018, publisher: Public Library of Science. [doi:10.1371/journal.pcbi.1008018](https://doi.org/10.1371/journal.pcbi.1008018).

[52] H. Tamura, K. E. Prokott, R. W. Fleming, Distinguishing Mirror From Glass: A “Big Data” Approach to Material Perception, *Journal of Vision* 22 (4) (2022) 4. [doi:10.1167/jov.22.4.4](https://doi.org/10.1167/jov.22.4.4).

[53] E. Watanabe, A. Kitaoka, K. Sakamoto, M. Yasugi, K. Tanaka, Illusory Motion Reproduced by Deep Neural Networks Trained for Prediction, *Frontiers in Psychology* 9, publisher: Frontiers (Mar. 2018). [doi:10.3389/fpsyg.2018.00345](https://doi.org/10.3389/fpsyg.2018.00345).

[54] P. Jaini, K. Clark, R. Geirhos, Intriguing Properties of Generative Classifiers, in: International Conference on Learning Representations (ICLR), 2024. [doi:10.48550/arXiv.2309.16779](https://doi.org/10.48550/arXiv.2309.16779).

[55] A. Gomez-Villa, K. Wang, C. A. Parraga, B. Twardowski, J. Malo, J. Vazquez-Corral, J. Van De Weijer, The Art of Deception: Color Visual Illusions and Diffusion Models, in: 2025 IEEE/CVF Conference on Computer Vision and Pattern Recognition (CVPR), 2025, pp. 18642–18652, iSSN: 2575-7075. [doi:10.1109/CVPR52734.2025.01737](https://doi.org/10.1109/CVPR52734.2025.01737).

[56] T. Karras, M. Aittala, J. Hellsten, S. Laine, J. Lehtinen, T. Aila, Training Generative Adversarial Networks with Limited Data, in: Proceedings of the 34th International Conference on Neural Information Processing Systems, NIPS ’20, Curran Associates Inc., Red Hook, NY, USA, 2020, pp. 12104–12114. [doi:10.48550/arXiv.2006.06676](https://doi.org/10.48550/arXiv.2006.06676).

[57] T. Karras, S. Laine, M. Aittala, J. Hellsten, J. Lehtinen, T. Aila, Analyzing and Improving the Image Quality of StyleGAN, in: 2020 IEEE/CVF Conference on Computer Vision and Pattern Recognition (CVPR), 2020, pp. 8107–8116, iSSN: 2575-7075. [doi:10.1109/CVPR42600.2020.00813](https://doi.org/10.1109/CVPR42600.2020.00813).

[58] R. W. Fleming, K. R. Storrs, Learning to See Stuff, *Current Opinion in Behavioral Sciences* 30 (2019) 100–108. [doi:10.1016/j.cobeha.2019.07.004](https://doi.org/10.1016/j.cobeha.2019.07.004).

[59] I. J. Goodfellow, J. Pouget-Abadie, M. Mirza, B. Xu, D. Warde-Farley, S. Ozair, A. Courville, Y. Bengio, Generative Adversarial Nets, in: Proceedings of the 28th International Conference on Neural Information Processing Systems - Volume 2, Vol. 2 of NIPS’14, MIT Press, Cambridge, MA, USA, 2014, pp. 2672–2680. [doi:10.48550/arXiv.1406.2661](https://doi.org/10.48550/arXiv.1406.2661).

[60] E. Richardson, Y. Alaluf, O. Patashnik, Y. Nitzan, Y. Azar, S. Shapiro, D. Cohen-Or, Encoding in Style: a StyleGAN Encoder for Image-to-Image Translation, in: 2021 IEEE/CVF Conference on Computer Vision and Pattern Recognition (CVPR), 2021, pp. 2287–2296, iSSN: 2575-7075. [doi:10.1109/CVPR46437.2021.00232](https://doi.org/10.1109/CVPR46437.2021.00232).

[61] T. Karras, S. Laine, T. Aila, A Style-Based Generator Architecture for Generative Adversarial Networks, in: 2019 IEEE/CVF Conference on Computer Vision and Pattern Recognition (CVPR), 2019, pp. 4396–4405, iSSN: 2575-7075. [doi:10.1109/CVPR.2019.00453](https://doi.org/10.1109/CVPR.2019.00453).

[62] W. Xia, Y. Zhang, Y. Yang, J.-H. Xue, B. Zhou, M.-H. Yang, GAN Inversion: A Survey, *IEEE Transactions on Pattern Analysis and Machine Intelligence* 45 (3) (2023) 3121–3138. [doi:10.1109/TPAMI.2022.3181070](https://doi.org/10.1109/TPAMI.2022.3181070).

[63] M. Kang, J.-Y. Zhu, R. Zhang, J. Park, E. Shechtman, S. Paris, T. Park, Scaling up GANs for Text-to-Image Synthesis, in: 2023 IEEE/CVF Conference on Computer Vision and Pattern Recognition (CVPR), 2023, pp. 10124–10134, iSSN: 2575-7075. [doi:10.1109/CVPR52729.2023.00976](https://doi.org/10.1109/CVPR52729.2023.00976).

[64] A. Jahanian, L. Chai, P. Isola, On the “Steerability” of Generative Adversarial Networks, in: International Conference on Learning Representations (ICLR), 2020. [doi:10.48550/arXiv.1907.07171](https://doi.org/10.48550/arXiv.1907.07171).

[65] Y. Shen, J. Gu, X. Tang, B. Zhou, Interpreting the Latent Space of GANs for Semantic Face Editing, in: 2020 IEEE/CVF Conference on Computer Vision and Pattern Recognition (CVPR), IEEE, Seattle, WA, USA, 2020, pp. 9240–9249. [doi:10.1109/CVPR42600.2020.00926](https://doi.org/10.1109/CVPR42600.2020.00926).

[66] X. Pan, A. Tewari, T. Leimkühler, L. Liu, A. Meka, C. Theobalt, Drag Your GAN: Interactive Point-based Manipulation on the Generative Image Manifold, in: ACM SIGGRAPH 2023

Conference Proceedings, SIGGRAPH '23, Association for Computing Machinery, New York, NY, USA, 2023, pp. 1–11. [doi:10.1145/3588432.3591500](https://doi.org/10.1145/3588432.3591500).

[67] Z. Wu, D. Lischinski, E. Shechtman, StyleSpace Analysis: Disentangled Controls for StyleGAN Image Generation, in: 2021 IEEE/CVF Conference on Computer Vision and Pattern Recognition (CVPR), 2021, pp. 12858–12867, iSSN: 2575-7075. [doi:10.1109/CVPR46437.2021.01267](https://doi.org/10.1109/CVPR46437.2021.01267).

[68] O. Tov, Y. Alaluf, Y. Nitzan, O. Patashnik, D. Cohen-Or, Designing an Encoder for StyleGAN Image Manipulation, ACM Trans. Graph. 40 (4) (2021) 133:1–133:14. [doi:10.1145/3450626.3459838](https://doi.org/10.1145/3450626.3459838).

[69] D. Bank, N. Koenigstein, R. Giry, Autoencoders, in: Machine Learning for Data Science Handbook: Data Mining and Knowledge Discovery Handbook, Springer International Publishing, Cham, 2023, pp. 353–374. [doi:10.1007/978-3-031-24628-9_16](https://doi.org/10.1007/978-3-031-24628-9_16).

[70] J.-Y. Zhu, P. Krähenbühl, E. Shechtman, A. A. Efros, Generative Visual Manipulation on the Natural Image Manifold, in: Computer Vision – ECCV 2016, Springer International Publishing, Cham, 2016, pp. 597–613. [doi:10.1007/978-3-319-46454-1_36](https://doi.org/10.1007/978-3-319-46454-1_36).

[71] M. J. P. V. Zuijlen, H. Lin, K. Bala, S. C. Pont, M. W. A. Wijntjes, Materials In Paintings (MIP): An interdisciplinary dataset for perception, art history, and computer vision, PLOS ONE 16 (8) (2021) e0255109, publisher: Public Library of Science. [doi:10.1371/journal.pone.0255109](https://doi.org/10.1371/journal.pone.0255109).

[72] J. Fišer, O. Jamriška, M. Lukáč, E. Shechtman, P. Asente, J. Lu, D. Sýkora, Stylit: Illumination-Guided Example-Based Stylization of 3D Renderings, ACM Trans. Graph. 35 (4) (2016) 92:1–92:11. [doi:10.1145/2897824.2925948](https://doi.org/10.1145/2897824.2925948).

[73] P. Litwinowicz, Processing Images and Video for an Impressionist Effect, in: Proceedings of the 24th annual conference on Computer graphics and interactive techniques, SIGGRAPH '97, ACM Press/Addison-Wesley Publishing Co., USA, 1997, pp. 407–414. [doi:10.1145/258734.258893](https://doi.org/10.1145/258734.258893).

[74] B. Burley, W. D. A. Studios, Physically-based Shading at Disney, in: Proceedings of ACM SIGGRAPH 2012, ACM, 2012, pp. 1–7.

[75] S. Panzeri, A. Treves, Analytical Estimates of Limited Sampling Biases in Different Information Measures, Network: Computation in Neural Systems 7 (1) (1996) 87–107, publisher: Taylor & Francis. [doi:10.1080/0954898X.1996.11978656](https://doi.org/10.1080/0954898X.1996.11978656).

[76] J. Runge, P. Nowack, M. Kretschmer, S. Flaxman, D. Sejdinovic, Detecting and Quantifying Causal Associations in Large Nonlinear Time Series Datasets, Science Advances 5 (11) (2019) eaau4996, publisher: American Association for the Advancement of Science. [doi:10.1126/sciadv.aau4996](https://doi.org/10.1126/sciadv.aau4996).

[77] L. van der Maaten, G. Hinton, Visualizing Data using t-SNE, Journal of Machine Learning Research 9 (86) (2008) 2579–2605.

[78] H. Ye, J. Zhang, S. Liu, X. Han, W. Yang, IP-Adapter: Text Compatible Image Prompt Adapter for Text-to-Image Diffusion Models, arXiv Preprint arXiv:2308.06721 (Aug. 2023). [doi:10.48550/arXiv.2308.06721](https://doi.org/10.48550/arXiv.2308.06721).

[79] R. Rombach, A. Blattmann, D. Lorenz, P. Esser, B. Ommer, High-Resolution Image Synthesis with Latent Diffusion Models, in: 2022 IEEE/CVF Conference on Computer Vision and Pattern Recognition (CVPR), 2022, pp. 10674–10685, iSSN: 2575-7075. [doi:10.1109/CVPR52688.2022.01042](https://doi.org/10.1109/CVPR52688.2022.01042).

[80] A. Radford, J. W. Kim, C. Hallacy, A. Ramesh, G. Goh, S. Agarwal, G. Sastry, A. Askell, P. Mishkin, J. Clark, G. Krueger, I. Sutskever, Learning Transferable Visual Models From Natural Language Supervision, in: Proceedings of the 38th International Conference on Machine Learning, Vol. 139 of Proceedings of Machine Learning Research, PMLR, 2021, pp. 8748–8763. [doi:10.48550/arXiv.2103.00020](https://doi.org/10.48550/arXiv.2103.00020).

[81] B. Ke, A. Obukhov, S. Huang, N. Metzger, R. C. Daudt, K. Schindler, Repurposing Diffusion-Based Image Generators for Monocular Depth Estimation, in: 2024 IEEE/CVF Conference on Computer Vision and Pattern Recognition (CVPR), 2024, pp. 9492–9502, iSSN: 2575-7075. [doi:10.1109/CVPR52733.2024.00907](https://doi.org/10.1109/CVPR52733.2024.00907).

[82] B. F. Labs, Flux, <https://github.com/black-forest-labs/flux> (2024).

[83] OpenAI, Gpt-4o image generation (gpt image 1), <https://openai.com/index/introducing-4o-image-generation/>, ai image generation model accessed via ChatGPT Plus (Mar. 2025).

[84] J. Chung, S. Hyun, J.-P. Heo, Style Injection in Diffusion: A Training-Free Approach for Adapting Large-Scale Diffusion Models for Style Transfer, in: 2024 IEEE/CVF Conference on Computer Vision and Pattern Recognition (CVPR), 2024, pp. 8795–8805, iSSN: 2575-7075. [doi:10.1109/CVPR52733.2024.00840](https://doi.org/10.1109/CVPR52733.2024.00840).

[85] H. Wang, M. Spinelli, Q. Wang, X. Bai, Z. Qin, A. Chen, InstantStyle: Free Lunch towards Style-Preserving in Text-to-Image Generation, arXiv Preprint arXiv:2404.02733 (Apr. 2024). [doi:10.48550/arXiv.2404.02733](https://doi.org/10.48550/arXiv.2404.02733).

[86] J. Guerrero-Viu, M. Hasan, A. Roullier, M. Harikumar, Y. Hu, P. Guerrero, D. Gutiérrez, B. Masia, V. Deschaintre, TexSliders: Diffusion-Based Texture Editing in CLIP Space, in: ACM SIGGRAPH 2024 Conference Papers, SIGGRAPH '24, Association for Computing Machinery, New York, NY, USA, 2024, pp. 1–11. [doi:10.1145/3641519.3657444](https://doi.org/10.1145/3641519.3657444).

[87] T. Y. Cheng, P. Sharma, M. Boss, V. Jampani, MARBLE: Material Recomposition and Blending in CLIP-Space, in: 2025 IEEE/CVF Conference on Computer Vision and Pattern Recognition (CVPR), 2025, pp. 13061–13071, iSSN: 2575-7075. [doi:10.1109/CVPR52734.2025.01219](https://doi.org/10.1109/CVPR52734.2025.01219).

[88] A. Hyvärinen, E. Oja, Independent Component Analysis: Algorithms and Applications, *Neural Networks* 13 (4) (2000) 411–430. [doi:10.1016/S0893-6080\(00\)00026-5](https://doi.org/10.1016/S0893-6080(00)00026-5).

[89] E. P. Simoncelli, B. A. Olshausen, Natural Image Statistics and Neural Representation, *Annual Review of Neuroscience* 24 (Volume 24, 2001) (2001) 1193–1216, publisher: Annual Reviews. [doi:10.1146/annurev.neuro.24.1.1193](https://doi.org/10.1146/annurev.neuro.24.1.1193).

[90] R. Zhang, P. Isola, A. A. Efros, E. Shechtman, O. Wang, The Unreasonable Effectiveness of Deep Features as a Perceptual Metric, in: 2018 IEEE/CVF Conference on Computer Vision and Pattern Recognition, 2018, pp. 586–595, iSSN: 2575-7075. [doi:10.1109/CVPR.2018.00068](https://doi.org/10.1109/CVPR.2018.00068).

[91] A. Krizhevsky, I. Sutskever, G. E. Hinton, ImageNet Classification with Deep Convolutional Neural Networks, in: *Advances in Neural Information Processing Systems*, Vol. 25, Curran Associates, Inc., 2012.

Supplementary Material: Style-Aware Gloss Control for Generative Non-Photorealistic Rendering

Santiago Jimenez-Navarro, Belen Masia, Ana Serrano

University of Zaragoza – I3A, Spain

S1. Training Dataset

As described in the main text (Sec. 3.2), we constructed a dataset for disentangling perceptual factors in non-photorealistic rendering. The dataset comprises 10,080 samples generated from the combination of three styles, 20 geometries, four illumination conditions, seven gloss levels, and six colors. Representative examples of each variation are shown in Fig. 13. For comparison, we also include the incremental gloss variations from the dataset of Subias et al. [32], which exhibits a less controlled progression of perceived gloss than our approach.

S2. Implementation Details

This section contains additional information regarding the training procedure followed to obtain the models analyzed in the main text.

S2.1. GAN-based Pipeline

We used as reference the official public implementation of StyleGAN2-ADA in Tensorflow (<https://github.com/NVlabs/stylegan2-ada>). Training was performed on a single NVIDIA Quadro RTX A6000 GPU in two steps: the first one for learning the general distribution of the dataset, using a learning rate of 1e-3, and a second to learn finer details, necessary to reconstruct artistic styles, with learning rate 1e-4. Both stages used batch size 16, a γ value of 10, ADA data augmentation with target 0.55, allowing augmentations on scale, rotation, anisotropy scaling, and fractional translation, and set path length regularization to 2.5. We trained during a total of 4,700 kimg (thousands of images), which took 216 GPU hours, for a final FID value of 28.4079. Finally, due to the 512x512 size of our training samples, the StyleGAN2-ADA generator consists of 16 convolution layers.

We also refer to the official implementation of the pixel2style2pixel encoder (<https://github.com/eladrich/pixel2style2pixel>).

This model was trained on an NVIDIA RTX 2080 Ti on a training subset that represented a 90% of the total training samples, and validated on the remaining 10%. We set the recommended balanced values of $\lambda_1=0.8$, $\lambda_2=1.0$, and $\lambda_3=0.005$, and a learning rate of 5e-5, for a final loss of 0.16645.

S2.2. Diffusion-based Pipeline

Our model builds on the *W+ Adapter* [18], the first method to condition a diffusion process on *W+* embeddings, originally applied for the domain of human faces. We introduce two key modifications to adapt this approach to our setup: (i) adopting Stable Diffusion XL 1.0 as the pretrained backbone model, leveraging its enhanced generative capacity over earlier Stable Diffusion versions, and (ii) implementing a transformer-based mapping network, which learns layer-wise attention patterns via positional encoding. The model was trained using PyTorch 2.0.1 and diffusers 0.23 on a single NVIDIA RTX A6000 GPU for six days, with learning rate of 1e-4, weight decay of 1e-4, batch size of 10, text drop rate of 0.3, and image drop rate of 0.05. Albedo map extraction was performed using Marigold [81], ControlNet weights are those from the diffusers library (<https://huggingface.co/diffusers/controlnet-canny-sdxl-1.0>), and we used stabilityai’s Stable Diffusion XL 1.0 model (<https://huggingface.co/stabilityai/stable-diffusion-xl-base-1.0>).

S3. Reconstruction Capabilities of the GAN-based Pipeline

We provide qualitative results demonstrating the reconstruction capabilities of the GAN-based pipeline, showing that it can (i) accurately recover the input appearance and (ii) closely reproduce the perceived gloss of the reference. Fig. 14 presents reconstructions of arbitrary samples spanning diverse generative factors, as

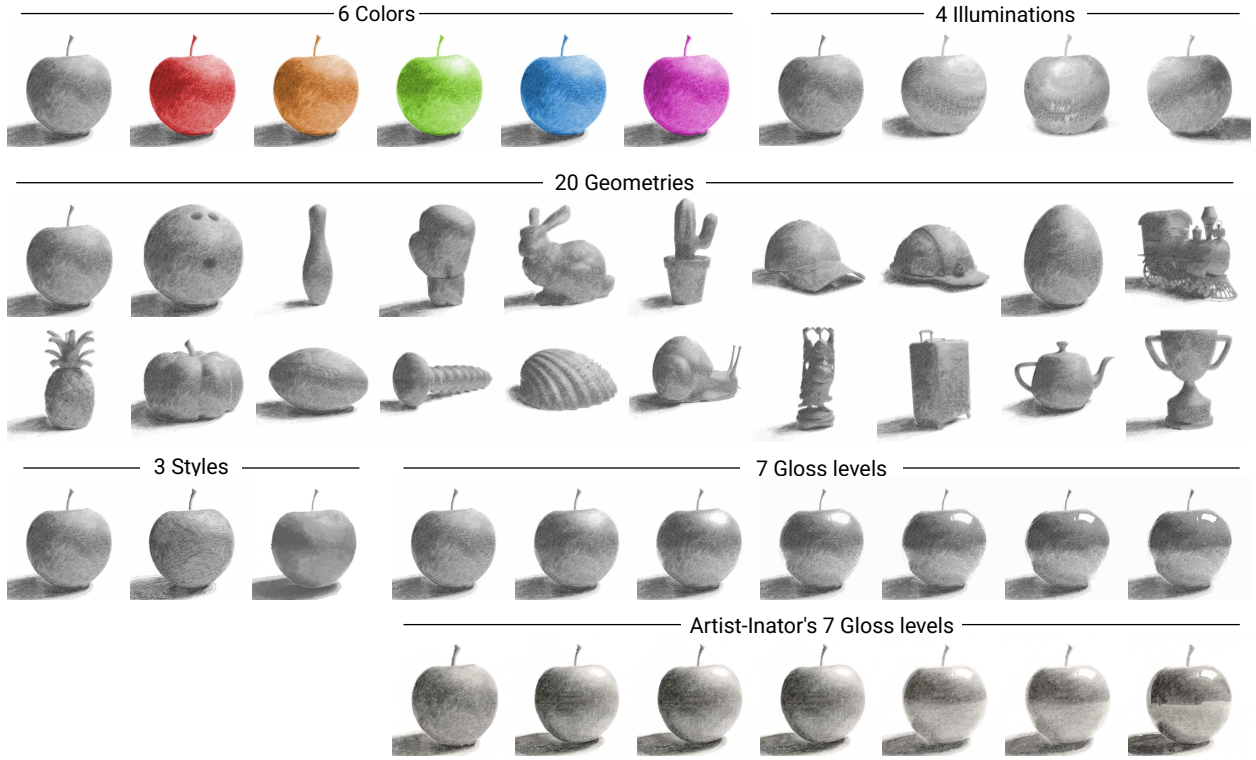


Figure 13: Representative samples of the five generative factors used to construct our custom dataset, showing one example for each color, illumination, geometry, style, and gloss level. For reference, samples from Artist-Inator [32] covering the seven gloss levels are included in the bottom right.

well as reconstructions across all seven gloss levels for a specific configuration.

S4. Internal Organization of the Latent Space: Additional Visualizations

We provide additional visualizations illustrating how the W^+ space naturally encodes an interpretable, hierarchical organization of perceptual features within its layer-wise architecture.

S4.1. Per-layer t-SNE Visualizations

For conciseness, only a subset of t-SNE visualizations was included in the main manuscript. Figs. 18, 19, 20, and 21 provide the complete set, confirming the trend illustrated in Fig. 6 of the main text: early layers ($W_{0..5}^+$) primarily encode *geometry* and *illumination*, as revealed by the emergence of distinct clusters when labeled accordingly, Layer 8 captures *style*, and the later layers ($W_{9..15}^+$) represent information related to *color*.

S4.2. Mutual Information Visualizations

The results in Fig. 22 reveal an information distribution across W^+ that is consistent with the qualitative observations in Fig. 6 of the main text, as obtained from the computation of the *Corr_MI* function described in Sec. 4.2.

S4.3. Internal Representations of Style Features

In this section, we investigate how and where style information is represented within the network. We first analyze how the StyleGAN generator progressively introduces the appearance cues that define the final image by visualizing intermediate outputs from the generator. These intermediate images are obtained from the tRGB layers attached after each resolution block. As shown in Fig. 15, the early resolutions (16x16 to 64x64) mainly encode global attributes such as geometry, illumination, and object placement. Style-specific cues become clearly visible at 128x128 resolution, which we argue is the minimum scale required to depict high-level details like brushstrokes. At later stages the network additionally refines gloss, specular highlights, and color. This gradual enrichment of features is reminiscent of how

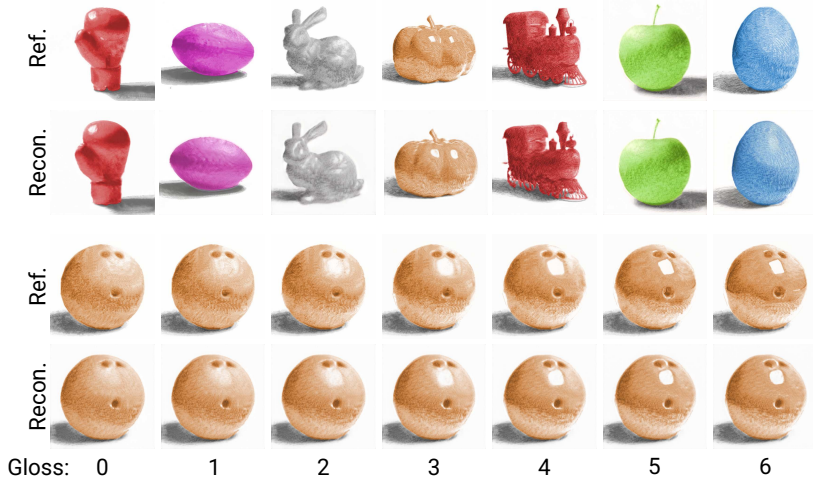


Figure 14: Evaluation of reconstruction capabilities of the trained pipeline. **Top:** reference (Ref.) and their respective reconstructions for samples with varied generative factors. **Bottom:** reconstruction of samples with progressively increasing glossy appearance.

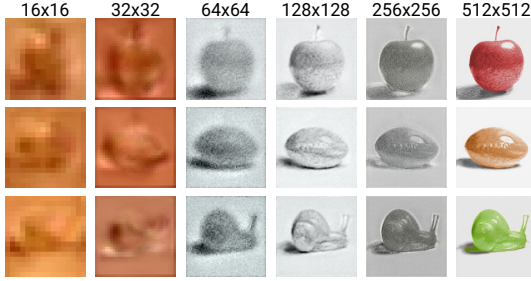


Figure 15: Intermediate tRGB visualizations per resolution. Initial visualizations capture coarse elements of the scene, such as object position, geometry or illumination, and later visualizations capture higher detail elements like style, specularity, or color.

a painter might proceed, beginning with coarse shapes and lighting and later adding stylistic details.

To further examine how style features are represented, we apply Independent Component Analysis (ICA) [88], inspired by prior work on natural image statistics [89]. ICA enables the discovery, through an optimization process, of independent basis functions that can explain the representation of a given signal (images in our case). We use visualizations of the three artistic styles at 128x128 resolution (Fig. 16, top left), and extract 64 independent basis functions through ICA (Fig 16, bottom left). We then convolve the learned kernels with painterly samples from our dataset to evaluate the type of information each basis function encodes, by inspecting the patterns that are highlighted (Fig 16, middle). Applying this analysis to three samples of different artistic styles (Fig. 16, right), we find that monochromatic kernels capture the largest amount

of style-related information. Interestingly, these kernels function much like edge detectors, indicating that the model has naturally developed filters aligned with the brushstroke structures of each style.

S5. Ablation on the Number of Styles: Additional Details

In the main text, we evaluate *latent space compactness* through the regularization metric proposed by Richardson et al. [60]. This metric is defined as the expected Euclidean distance between an encoded latent vector and the generator’s average latent vector $\bar{\mathbf{w}}$, formulated as specified in Eq 1.

$$\text{Reg} = \mathbb{E}_{x \sim P_{\text{data}}} [\|E(x) - \bar{\mathbf{w}}\|_2] \quad (1)$$

Furthermore, we compute Perceptual Path Length to assess the *smoothness and continuity* of latent spaces. PPL measures changes in the generated image resulting from a small step ϵ in the latent space. We compute PPL using linear interpolation between the w^+ codes of real samples. Specifically, we employ the traditional step size of $\epsilon = 10^{-4}$ and utilize the LPIPS metric [90] with an AlexNet backbone [91], which is better suited for our non-photorealistic setup than the standard VGG [26]. The metric is computed as specified in Eq 2, where w_t^+ represents a point along the interpolation path between two latent codes, and $G(\cdot)$ represents the *Generator* network [61].

$$\text{PPL} = \frac{1}{\epsilon^2} \mathbb{E}[\text{LPIPS}(G(w_t^+), G(w_{t+\epsilon}^+))] \quad (2)$$

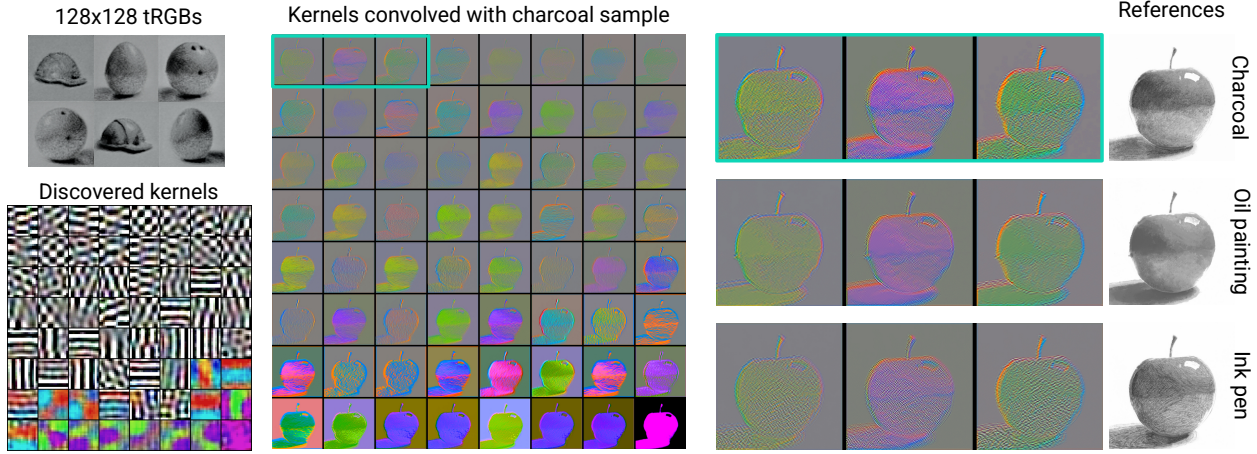


Figure 16: **Top left:** representative samples of the 128x128 tRGB representations to train the ICA model. **Bottom left:** 64 kernels discovered with ICA, using patch size 16x16. Kernels are ordered with respect to their variance on changes in style. **Middle:** result of convolving the discovered kernels with a gray charcoal apple. **Right:** top three most informative kernels convolved with samples of all the three styles.

For fairness, all the four models used in this ablation study have been trained the same number of epochs, and we compute metrics on test samples.

S6. Diffusion Conditioning via Text Prompt

The proposed diffusion-based pipeline supports varying levels of granularity in conditioning on spatial information for geometry and color. Fig. 17 presents results obtained using only text prompts to synthesize new images. As expected, this setup introduces variability in the generated geometries. However, the strong disentanglement properties of the trained adapter enable controlled modification of individual scene factors while preserving the others.

S7. User Study: Additional Details

Demographics The user study was conducted with 22 participants (mean age 28.9 ± 9.3 years, 7 female). Regarding prior experience in *Computer Graphics*, one participant reported no experience, one had beginner-level knowledge, one had intermediate-level knowledge, 17 reported advanced knowledge, and two identified as experts. In terms of prior experience in *Art*, one participant reported no experience, 15 identified as beginners, five reported intermediate knowledge, and one identified as an expert.

Execution of Reference Methods We provide here a detailed description of the execution of the reference methods presented in Fig. 13 (main text), three of which—DEADiff, InstantStyle, and Artist-Inator—were also included in the user study.

- **GPT Image 1** [83] was accessed via the ChatGPT interface (<https://chatgpt.com/>). For geometry guidance, the *geometry reference* image was directly uploaded. An example prompt used for image synthesis is: “*Stylize this image in orange ink pen style. Make it very glossy.*” Further analysis of gloss conditioning alternatives is provided in Sec. S8.
- **FLUX** [82] was executed through the *FLUX Style Shaping* space (<https://huggingface.co/spaces/multimodalart/flux-style-shaping>, last accessed Sept. 2025), which implements FLUX_dev and enables style transfer with reference images.
- **StyleID** [84] was run using the official implementation (<https://github.com/jiwoogit/StyleID>, last accessed Sept. 2025), with both the reference style/gloss and reference geometry images provided as input.
- **DEADiff** [29] was configured using its official repository (<https://github.com/bytedance/DEADiff>, last accessed Sept. 2025). The appropriate reference inputs were provided, and weights were tuned to optimize results.
- **InstantStyle** [85] was run with the official implementation (<https://github.com/instantX-research/InstantStyle>, last accessed Sept. 2025). We used pairs of images for geometry and for style/gloss reference, and further guided the generation with text prompts.

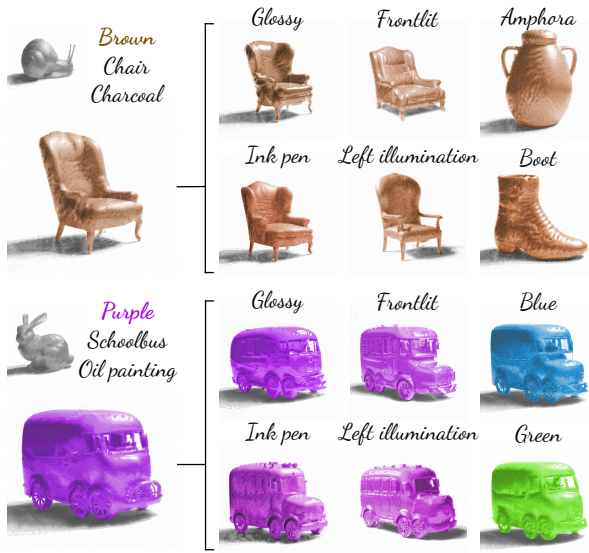


Figure 17: Results of the pipeline when guiding geometry with text prompt. **Left:** result of transferring the style and gloss level from a reference image to a geometry whose color and illumination are defined by text prompt. **Right:** modifying a single factor leads to isolated appearance changes in the specified factor, leaving the remaining ones unchanged.

- **Artist-Inator** [32] was executed following the steps in the official repository (<https://github.com/dsubias/Artist-Inator>, last accessed Sept. 2025). Geometry was guided via a Canny edge map, while style, gloss, and color were conditioned through text prompts.

Procedure For each pair of *geometry* and *style & gloss* reference images, participants were asked to rank the outputs of the four style transfer methods under evaluation. To ensure accurate assessment of fine details—particularly important for styles such as *ink pen*—participants were allowed to zoom in on the images. Both the order of the questions and the order of the alternatives within each question were randomized. Fig. 23 illustrates the interface from a participant’s perspective.

S8. Gloss Traversals with GPT Image 1

Given the limited fine-grained control over perceptual features such as gloss in general-purpose T2I models, we evaluated a set of alternative prompting strategies to determine which was best understood by such models. As illustrated in Fig. 24, we tested: (i) percentages of gloss, ranging from 0% (very matte) to 100% (very glossy), (ii) numerical labels from 0 to 6, following the

same principle, and (iii) textual descriptions of seven gloss levels as proposed by Subias et al. [32]. Among these, option (iii) proved the most effective for conditioning T2I models on gloss appearance, which we hypothesize is due to descriptive text being more easily interpreted by the text encoder.

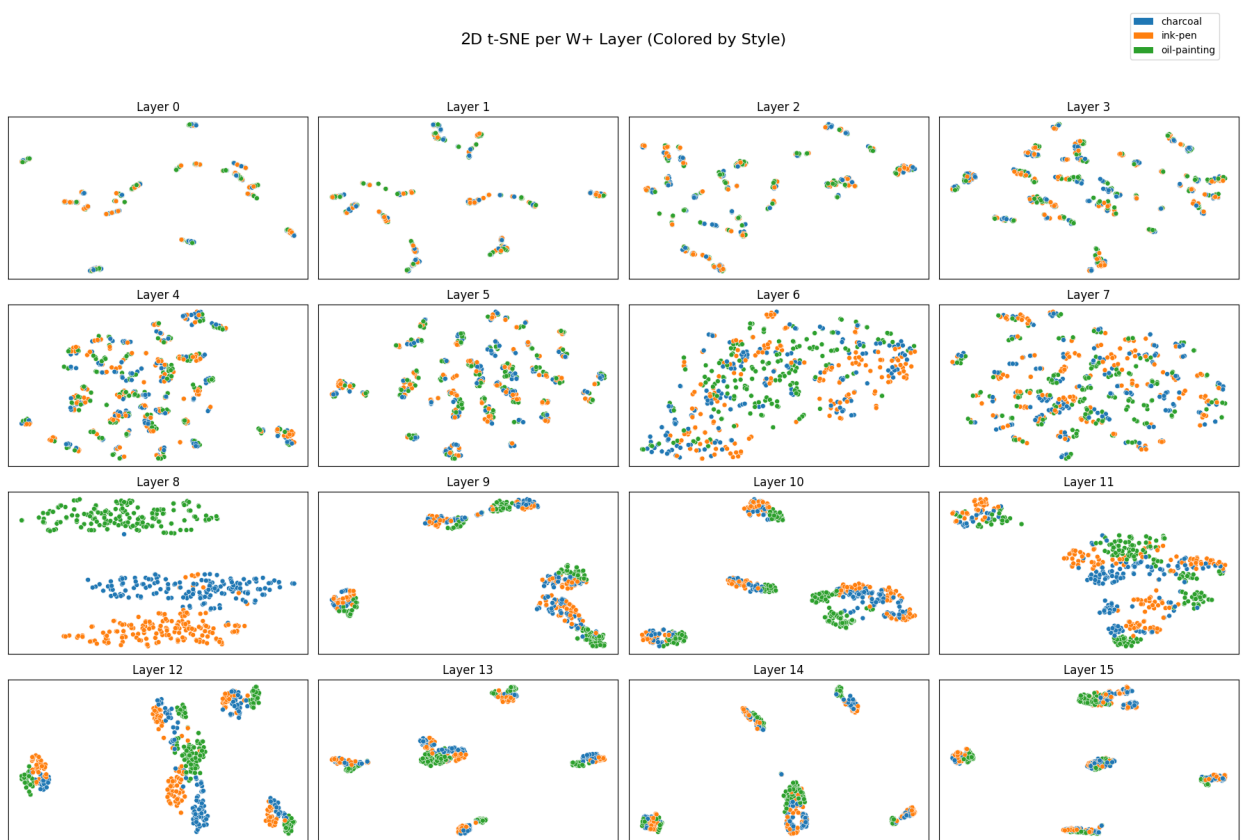


Figure 18: Complete t-SNE visualization of the 16 layers in the $W+$ space. Samples are colored according to their **style** label, showing that this factor is most prominently captured in Layer 8.

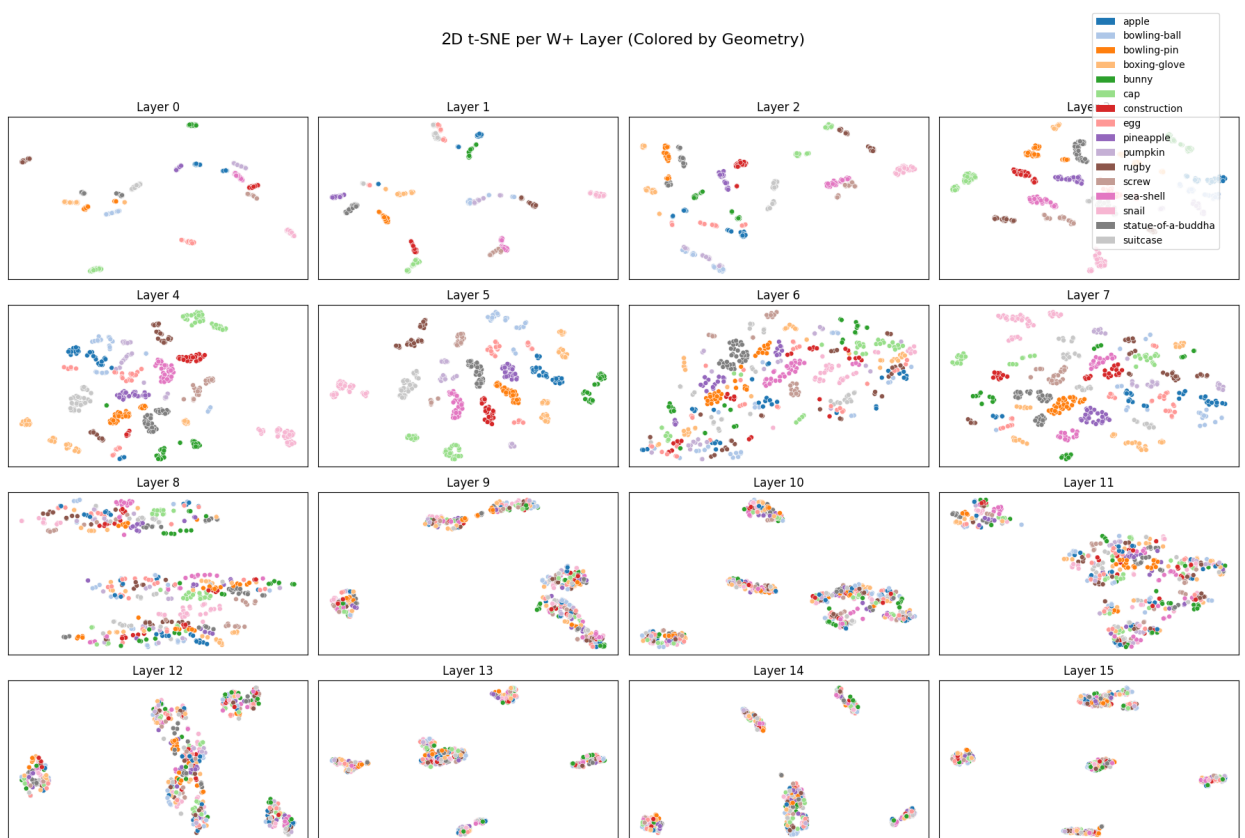


Figure 19: Complete t-SNE visualization of the 16 layers in the W^+ space. Samples are colored according to their **geometry** label, showing that this factor is mainly captured in early layers of the space ($W_{0.5}^+$).



Figure 20: Complete t-SNE visualization of the 16 layers in the W^+ space. Samples are colored according to their **illumination** label, showing that this factor is mainly captured in early layers of the space ($W_{0..5}^+$).

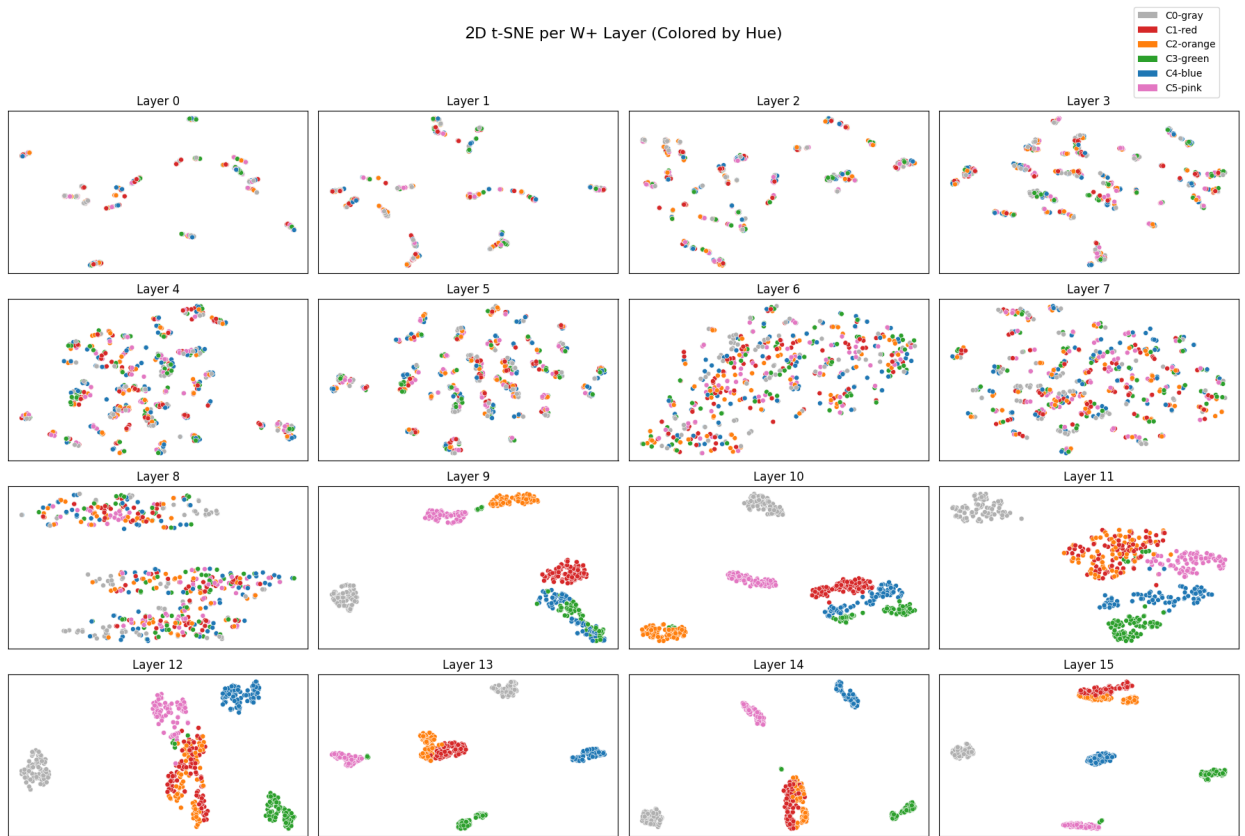


Figure 21: Complete t-SNE visualization of the 16 layers in the W^+ space. Samples are colored according to their **color** label, showing that this factor is mainly captured in late layers of the space ($W_{9..15}^+$).

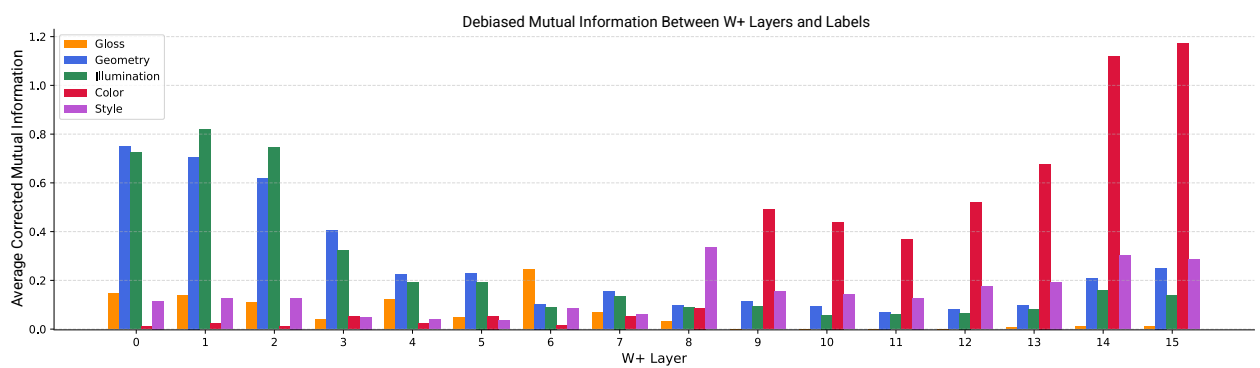


Figure 22: Corrected per-layer Mutual Information scores shows how generative factors are adequately distributed over W^+ layers.

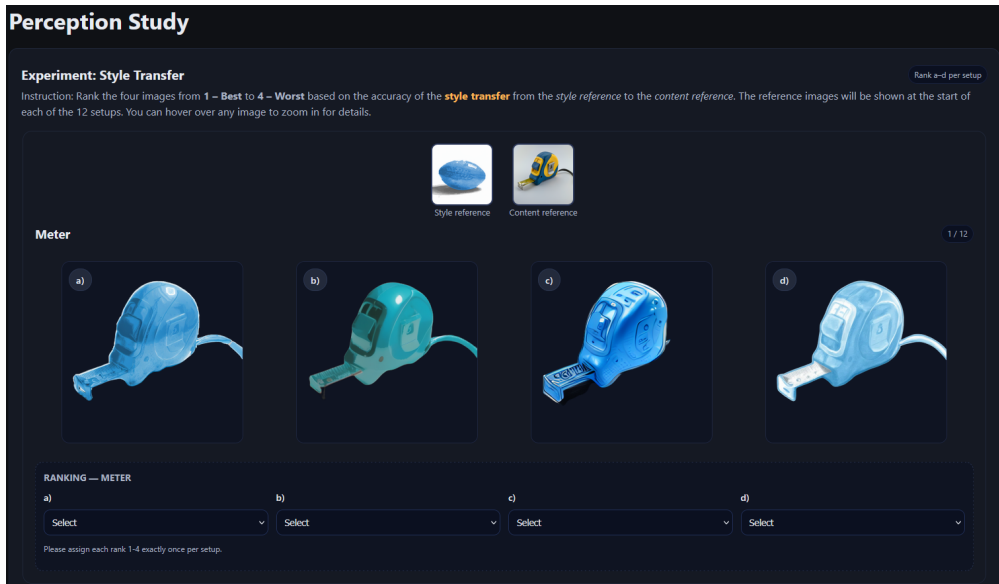


Figure 23: Screenshot of the web-based user study interface used to evaluate the performance of four methods: DEADiff, InstantStyle, ArtistInator, and ours.

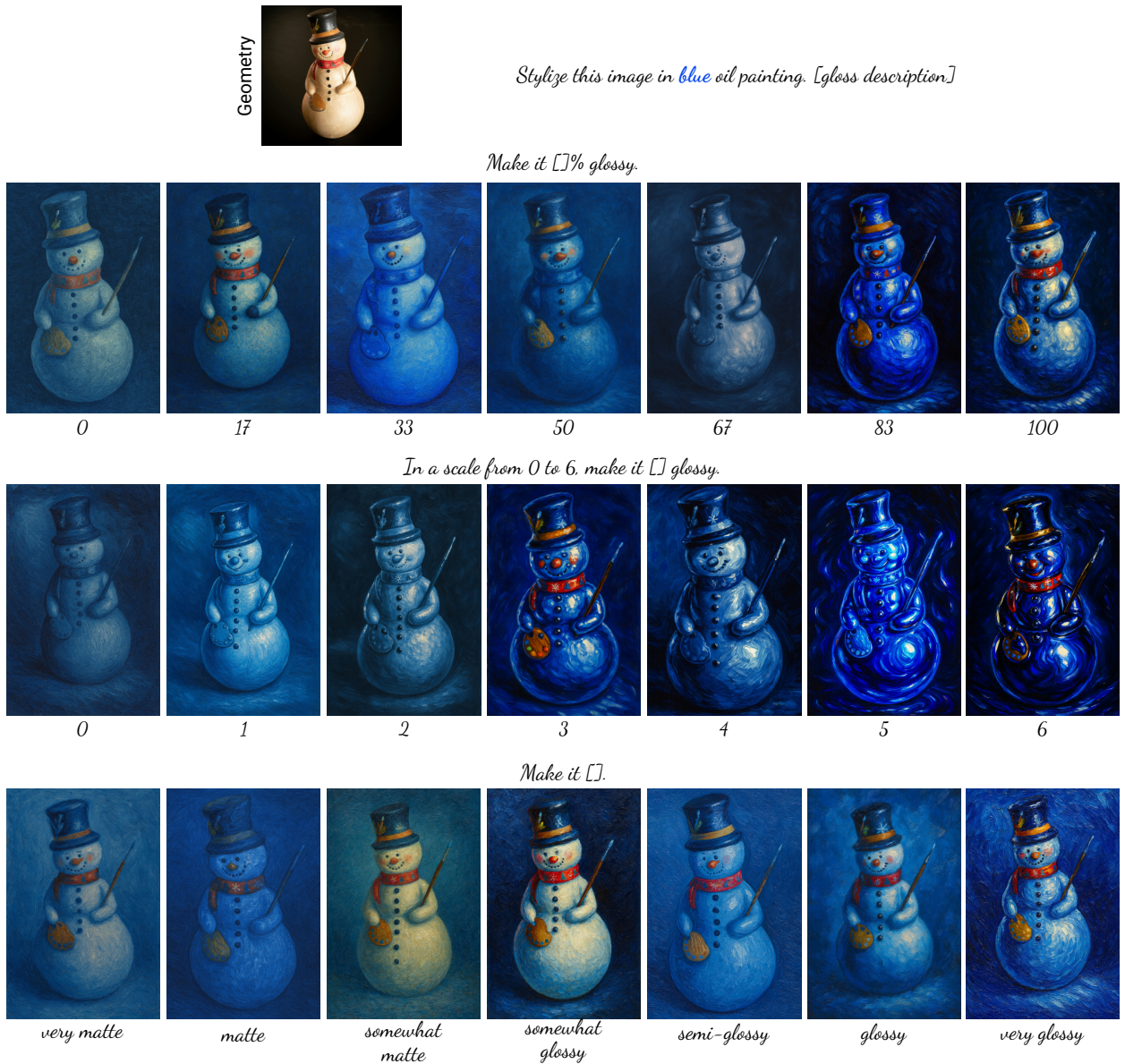


Figure 24: Qualitative comparison of style transfer results generated for the same geometry while varying the definition of gloss appearance. Three prompting strategies are tested: percentages (top), numerical labels (middle), and textual descriptions of gloss levels as proposed by Subias et al. [32] (bottom).